# METAL DUST CLOUD DISTRIBUTION CHARACTERIZATION THROUGH IMAGE ANALYSIS

A Thesis
presented to
the Faculty of California Polytechnic State University,
San Luis Obispo

In Partial Fulfillment
of the Requirements for the Degree
Master of Science in Mechanical Engineering

by
Shelby Lampshire
June 2021

COMMITTEE MEMBERSHIP

| | |
|---|---|
| TITLE: | Metal Dust Cloud Distribution Characterization Through Image Analysis |
| AUTHOR: | Shelby Lampshire |
| DATE SUBMITTED: | June 2021 |
| COMMITTEE CHAIR: | Andrew Davol, Ph. D<br>Professor of Mechanical Engineering |
| COMMITTEE MEMBER: | Giri Gopalan, Ph. D<br>Assistant Professor of Statistics |
| COMMITTEE MEMBER: | Richard Emberley, Ph. D<br>Assistant Professor of Mechanical Engineering |

ABSTRACT

Metal Dust Cloud Distribution Characterization Through Image Analysis

Shelby Lampshire

With the increasing development of metal additive manufacturing technology, the present need for accurate explosivity testing of high density and exotic metal powders is under active research. The accuracy of such tests depends upon the uniformity of the dust dispersion within the testing chambers during ignition. There is a need for further research to understand the dust cloud dispersion process in order to determine the best time for ignition. This study explores a methodology of using high-speed footage and image analysis to characterize the uniformity of a dust cloud temporally that future applications may build upon.

This thesis consisted of the experimental methods used to generate a dust cloud for image acquisition and an in-depth study of processing pixel data in MATLAB to determine points of highest dust cloud uniformity. The image analysis process was applied to the generated footage and the results were assessed through visual means. The analysis was also applied to dust cloud footage generated by Lawrence Livermore National Laboratory on a transparent replica of a modified ANKO 20-L explosivity testing apparatus. The image analysis methodology proved to offer a promising means of determining dust distribution uniformity as it relates to the timing of explosivity ignition.

ACKNOWLEDGMENTS

I would like to share my sincere thanks and appreciation to my committee chair, Dr. Andrew Davol, for your endless support and encouragement throughout this thesis project. You provided continuous insight and were always there to advise me in the right direction. I would also like to thank my other committee members, Dr. Richard Emberley and Dr. Giri Gopalan for always pushing me to keep improving my work. You both provided essential feedback and invaluable expertise during this project.

Thank you to Lawrence Livermore National Laboratory for supporting this thesis opportunity that has taught me so much. To the individuals at LLNL, specifically Mike Ades and Matt Roberts, thank you so much for providing guidance throughout this process.

Thank you to Jeff Van Kleeck for sharing your photography expertise and providing resources that aided in the success of this project. Thank you to Eric Pulse for the never-ending patience you have shown me throughout the years and during this project.

I have endless thanks to give to the Cal Poly Mechanical Engineering Department for providing me with everything I needed to be successful as an undergraduate and graduate engineering student. Even during a pandemic, I could trust that I would have all the resources necessary to complete this thesis project.

Finally, I would like to thank my loving friends and family who have been by my side, motivating and encouraging me to the finish line. I am so grateful to have had your immense support.

TABLE OF CONTENTS

Page

# LIST OF TABLES

Table Page

# LIST OF FIGURES

# 1 INTRODUCTION

Metal powders have become more widely used with the development and implementation of additive manufacturing (AM). AM is defined by ASTM as "a process of joining materials to make objects from 3D model data, usually layer upon layer, as opposed to subtractive manufacturing methodologies." As a manufacturing process, AM relies on the availability of safe, reliable materials. This can include a wide variety of materials including metals, ceramics, polymers, composites, and biological materials. Many of the metallic AM systems, including powder bed and powder fed systems, require the metal to be in powder or dust form in order to operate. [1]

## 1.1 Dangers of Combustible Dust

Unfortunately, safety hazards associated with working with combustible materials, like many metals, exist in powder form. The small particle size of any combustible powder increases the ignition sensitivity and explosion severity due to the increased surface area available for combustion relative to their weight. Many incidents have occurred that have led to fatalities, injuries, and equipment damage. According to a 2006 study by the U.S Chemical Safety Board, at least 281 combustible dust explosions occurred between 1980 and 2005 in the United States [2].

For a dust explosion to occur, conditional criteria must be met. In other words, five elements must be present simultaneously in order for a dust explosion to take place. First, combustible dust, which is the fuel (1), and oxygen (2) must be present. Additionally, the fuel must be dispersed in suspension, (3) which results in the dust burning rapidly. There must be an adequate ignition source to start the reaction, (4) and finally, the combustion must be confined, which allows pressure buildup (5). Figure 1-1 shows this concept and all these necessary components in the form of a dust explosion pentagon. [3]

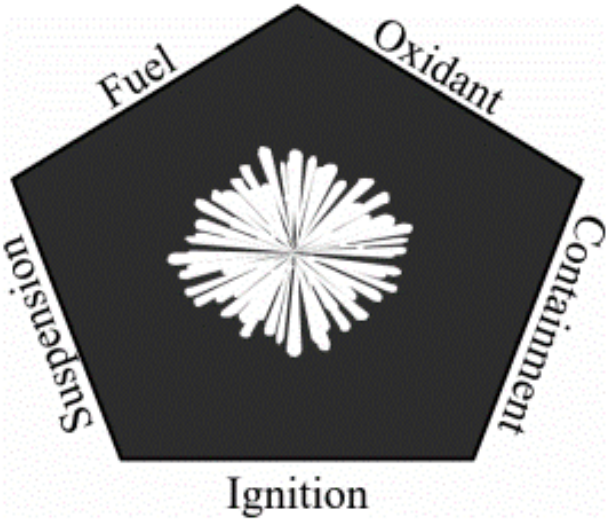


Figure 1-1. Diagram of the explosion pentagon, which shows the elements required for a dust explosion to take place [3].

Other factors that contribute to the explosiveness of dusts includes moisture content, ambient humidity, oxygen availability, particle shape, and the dust concentration in air. The intensity of an explosion can be evaluated from a certain powder's explosibility index, $K_{st}$. This measures the relative explosion severity compared to other dusts. This is just one powder explosivity characteristic that can be measured for a specific powder.

In order to properly evaluate the hazards of working with combustible dust, measuring properties for that dust at the specific conditions that they will be used in is a key step in addressing those hazards. Testing processes exist to measure these explosivity characteristics that are employed for this very problem to better understand certain dust materials at various operating conditions [2].

## 1.2 Dust Explosivity Characteristic Testing

The procedure for determining specific dust material explosivity characteristics is often done by dispersing a known mass of the dust into a closed volume chamber and igniting the dust with known parameters. Chambers like the PRL 20-L, Siwek 20-L, Anko 20-L, and the Fike 1-$m^3$ test

chambers measure characteristics such as maximum explosion pressures, maximum rates of pressure rise, and minimum explosible concentrations [4]. These explosibility characteristics are important to know when working with specific dust materials especially under any of the conditions that may produce combustion. An example of a testing apparatus for this purpose can be seen in Figure 1-2. The most commonly measured explosivity characteristics are specified in Table 1-1.

However, an important assumption that these tests make when characterizing the explosivity of a material is that the dust cloud formed in the chamber is uniform [5]. Since the distribution of the cloud effects the accuracy of the test results, it is important to study this spatial distribution and determine ways of verifying and understanding the spatial and temporal uniformity in a dust cloud.

Figure 1-2. 20-Liter ANKO sphere apparatus for determining explosion characteristics of dust clouds [6].

Table 1-1. Measured properties of combustible dust [2].

| Property | Definition | ASTM Test Method | Application |
|---|---|---|---|
| $K_{St}$ | Dust deflagration index | ASTM E 1226 | Measures the relative explosion severity compared to other dusts. |
| $P_{max}$ | Maximum explosion overpressure generated in the test chamber | ASTM E 1226 | Used to design enclosures and predict the severity of the consequence. |
| $(dp/dt)_{max}$ | Maximum rate of pressure rise | ASTM E 1226 | Predicts the violence of an explosion. Used to calculate $K_{St}$. |
| MIE | Minimum Ignition energy | ASTM E 2019 | Predicts the ease and likelihood of ignition of a dispersed dust cloud. |
| MEC | Minimum explosible concentration | ASTM E 1515 | Measures the minimum amount of dust, dispersed in air, required to spread an explosion.<br><br>Analogous to the lower flammability limit (LFL) for gas/air mixtures. |
| LOC | Limiting oxygen concentration | ASTM standard under development | Determines the least amount of oxygen required for explosion propagation through the dust cloud. |
| ECT | Electrostatic charging tendency | No ASTM standard | Predicts the likelihood of the material to develop and discharge sufficient static electricity to ignite a dispersed dust cloud. |

## 1.3 Previous Work

Lawrence Livermore National Laboratory, or LLNL, has been performing cutting edge research in additive manufacturing. They are increasing their additive manufacturing capabilities by exploring different metal powders to use and need to determine the explosivity of these powders to ensure the safety of operating with them. A 20-L ANKO explosivity testing apparatus was acquired and was found to not be effective when testing dense powders. In order to improve this capability, they have made modifications to the dispersion nozzle on the vessel. A transparent replica of the modified ANKO testing chamber was built to visually inspect spatial uniformity of the dust cloud formed after their modifications. High-speed footage was acquired to do this.

Presently, LLNL wants to better characterize the powder cloud created after their modifications to ensure the accuracy of the device. Understanding the distribution of the powder cloud during this explosivity testing is an important step in this process.

This project aims to aid in this effort with the inclusion of an image analysis methodology to characterize dust distribution and develop a way to determine the optimum ignition time of a dust cloud formation. Although this experimental setup exists, this transparent ANKO chamber is not available for use in this project. However, footage of dust distribution from this setup is used for application of the image analysis after development.

## 1.4 Objective

The objective of this thesis is to develop a methodology of characterizing the spatial and temporal distribution of the powder cloud visually through image analysis. This includes the generation of an enclosed dust cloud that is filmed using a high-speed camera. The image analysis methodology uses the frames in this footage to extract a quantitative assessment of the distribution characteristics of a dust cloud over time. Additionally, the method uses input criteria on the data to provide identification of the frame numbers, and resulting time period, that has the most optimized dust cloud in the footage.

# 2 LITERATURE REVIEW

## 2.1 Relevant Research Studying Dust Cloud Distribution

Many methods have been researched for analyzing dust cloud dispersion and density for the application of determining the hazards associated with combustible dust from past and current research. This has included the use of optical density probes, computational fluid dynamics modelling, and visual analysis.

### 2.1.1 Optical Density Probes

Extensive research has been done by Pittsburg Research Lab and the Bureau of Mines involving the use of optical density probes to measure the effectiveness of dust dispersion. Optical density probes operate on the principle of light attenuation by measuring the transmittance of light or radiation through dust clouds. A simple single-path-length probe consists of a light source and a photodetector at a known distance from one another. The transmittance of light can be used to determine the mass concentration in a cloud [7]. A single-path-length optical density probe schematic is seen in Figure 2-1. The effectiveness of dust dispersion in explosibility chambers has been studied by positioning various optical density probes within a chamber and measuring and comparing optical transmittance results [5].

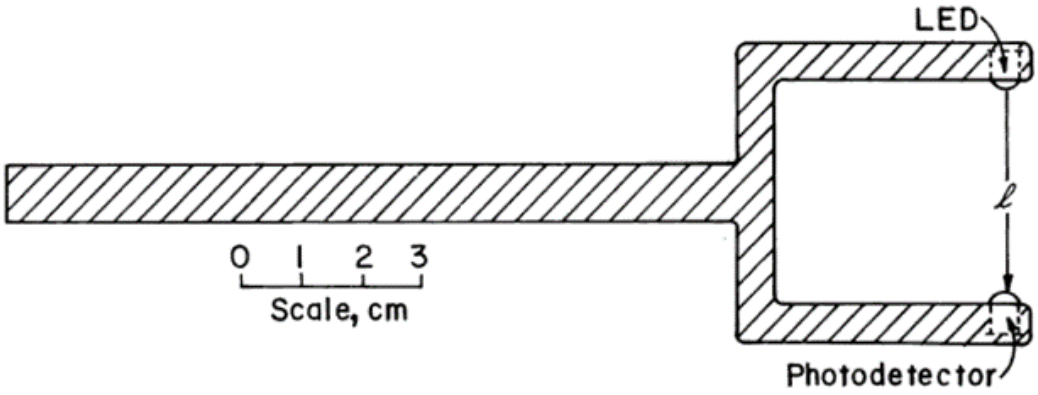


Figure 2-1. Single-path-length optical dust probe [7].

### 2.1.2 CFD Modelling

Another way of studying the dust dispersion in explosibility chambers has been to develop 3-D computational fluid dynamics models. Di Benedetto et al. have described the turbulent flow inside a 20-L chamber with a common rebound nozzle and the effects on dust concentration distribution through CFD analysis [8]. They found that turbulent vortex structures are generated in the 20 L spherical chamber which contribute to nonuniformity of the dust concentration. Additionally, the fluid flow is found to become asymmetric due to the dust presence and the effects of particle sedimentation. Their model has been validated by measurements of time histories of pressure and root mean square velocities known from literature.

### 2.1.3 Visual Analysis

Much like what this project is focusing on, another way that past research has studied the dispersion process of dust clouds is through visual experiments and image analysis. This was specifically done by Du et al. in a transparent Siwek 20-L chamber with carbonaceous dust. This dispersion system is similar to LLNL's transparent ANKO 20-L chamber and allows high-speed footage to be taken to study the resulting dust cloud. This research includes carrying out analysis based on light transmission data from the pixels in the footage images. It also includes studying the dispersion behavior with different nominal dust concentrations used. The results found that there are three defined stages of dust dispersion in the Siwek chamber: a fast injection stage, a stabilization stage, and a particle sedimentation stage. They also found that in the stabilization stage, the best dust cloud uniformity is attained when the deviation of transmission data at different enclosure locations are at a minimum [9]. This result is used as an assumption for the present study.

The testing setup used by Du et al. is seen in Figure 2-2 to be different than the experimental testing setup in the present study. However, this thesis project setup uses a similar

backlighting arrangement, where the high-speed camera faces the enclosure with a light shining straight through the other side. Additionally, pixel grayscale intensities are used in both studies to determine light transmission and this measurement is assumed to correspond to dust concentration. The Siwek study analyzes different pixel matrix regions in the enclosure to compare data to check for uniformity [9]. This technique is also used in the present study to determine dust presence as well as uniformity across the enclosure.

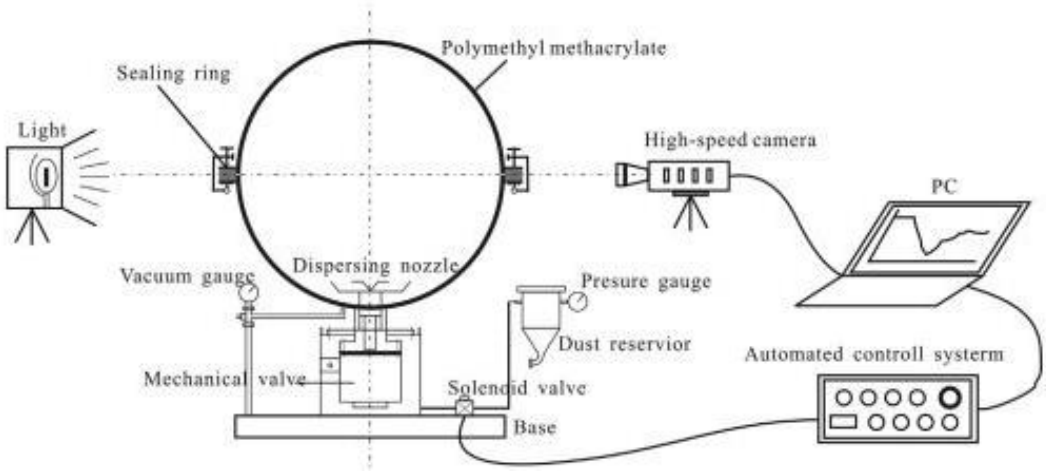


Figure 2-2. Schematic diagram of transparent Siwek experimental setup performed by Du et al. [9].

## 2.2 Image Analysis Methods

In addition to the image analysis methods used by Du et al. in the transparent Siwek 20-L chamber, other research using image analysis is relevant to reference in the context of this project. Image analysis methods are implemented to study the distribution of many different materials in many different applications. Research done by Daumann et al. uses image analysis to determine the mixing efficiency of a discontinuous powder mixer by tracking powder flow through color tracer particles. Ultramarine blue tracer particles were used in this study to create a color contrast with the base cement material. This blue color component in the images was then separated using color intensities and thresholds were applied to aid in determining the uniformity of the blue particles in the base particles [10]. This research shows how color components can

help aid in spatial distribution image analysis if applicable. Although color images are not utilized in the present study, this is an interesting image analysis method used in literature.

Research done by Bedggood and Metha use image analysis, specifically pixel intensity cross correlation, to map the cellular flow velocity in human retinal networks [11]. Techniques that are explored in this present study were also implemented in this flow velocity research. These methods include the use of pixel intensity normalization by division and background subtraction. Background subtraction was implemented in this flow velocity study to remove extraneous background information. Although this is a different application, this preprocessing step has the same objective in both this research and the present study.

A very applicable research study has been done by Zhao and Ambrose, which implements image analysis and light attenuation theory to determine dust cloud concentration with a rapid response time. The objective of this research was to develop a two-target method for measuring the concentration of a dust cloud in both open and confined spaces of cornstarch, corn dust, and sawdust. The light extinction coefficient was used, which represents the rate of diminished transmitted light through a cloud and is linearly related to the dust concentration. This literature was successful in applying light attenuation principles and was verified by optical density probe concentration results. [12] Similar light attenuation theory and corresponding assumptions are used in this present study.

# 3 METHODS

## 3.1 Experimental Setup and Design

The goal of the present experiment is to achieve a powder cloud in a safe manner that can be seen clearly and recorded using a high-speed camera. The ideal experimental setup is to replicate the ANKO test vessel in a transparent manner, much like what had been done at LLNL. However, for simplification and safety on the California Polytechnic State University San Luis Obispo campus, a transparent drop test fixture is used instead. The information and the image processing program developed in this thesis using the powder cloud from this drop test can then be applied LLNL's setup, as well as other future applications.

In order to develop this image analysis program, the most essential features in the testing setup are adequate and consistent light, an enclosure with a visible and varying dark powder cloud, and a means to record the cloud.

### 3.1.1 Drop Test Design

The testing apparatus consists of a clear acrylic cylinder with a diameter of 10 inches and a height of 24 inches. A testing sieve is suspended from the top, inside the enclosure, in which the powder is placed into. At the bottom of the cylinder, a collection pan is pressed up on the cylinder by the frame to catch the falling powder. This allows the metal powder to drop from the sieve, form a cloud, and fall into the collection pan while always contained in the enclosure.

At the top, the cylinder is sealed with a flange, rubber ring, and acrylic plate sandwiched and clamped together. At the sides, the cylinder is attached to a rigid frame which holds it above the tabletop. The rigid frame is necessary to keep the enclosure's position consistent for taking footage as the sieve moves around to release the powder. The raised position of the cylinder allows access to the powder in the collection pan by releasing the bottom beam holding the pan up. The powder is then reused and the enclosure inside walls are cleaned of any powder residue obstructing the camera view.

The powder release arrangement consists of a suspended testing sieve with mesh size openings of 0.075 mm. The sieve is suspended by three springs inside of the enclosure. Two small motors are magnetically attached to the cylinder wall above the sieve. Cams on the motor shafts tap the side of the sieve when activated and this motion releases the stagnant powder sitting inside. This design allows for the powder drop test to be operated outside of the sealed enclosure without manual sieve shaking. The testing apparatus is seen in Figure 3-1 and Figure 3-2. Appendix A includes detailed information on the sieve, motors and other equipment used. Additionally, other design considerations for cloud formation are referenced in Appendix B.

This drop test results in rhythmic clouds of falling dust within the transparent chamber that matches the motor rpm tap releasing the powder in the sieve. The clouds are unique from one another and generally not uniform. However, clouds of different distributions are generated with this design and produce the test footage required to develop a robust image analysis program.

Figure 3-1. Experimental enclosure and framing setup.

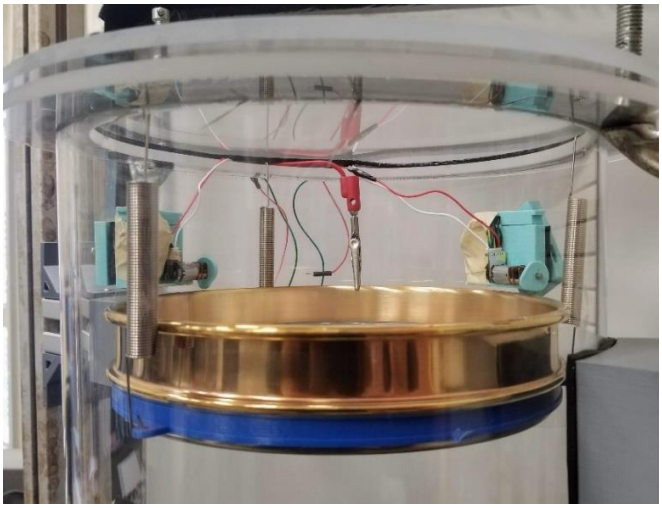

Figure 3-2. Powder release sieve arrangement showing the motors and cams that tap the sieve to drop the powder repeatedly. The metal sieve is grounded to discharge any static buildup in the sieve and powder.

### 3.1.2 Camera and Lighting Setup

The generated cloud within the enclosure is filmed using a Phantom v310 high-speed camera and a Sigma EX DG Macro lens. The lens faces the wall of the transparent cylinder with the light placed on the other side. The lighting consists of a 150-watt fluorescent bulb within a large soft box to diffuse the light across the enclosure area in the frame. See Appendix A for details of equipment used. While acquiring footage, no other artificial light is used and the windows in the testing space are covered to minimize any outside light or glares affecting the footage.

The resulting footage from the tests are backlit, grayscale images of falling powder. The number of images acquired in a single take ranges from approximately 300 to 1000 frames depending on how long the test is. With the specified high-speed camera, only grayscale images are produced, and individual particles are not distinguishable, however, the necessary details of the powder cloud are visible. The grayscale images have a resolution of 600x800 pixels. The setup and a resulting frame from testing is seen in Figure 3-3 and Figure 3-4.

Figure 3-3. Camera, test apparatus, and backlighting setup for footage acquisition.

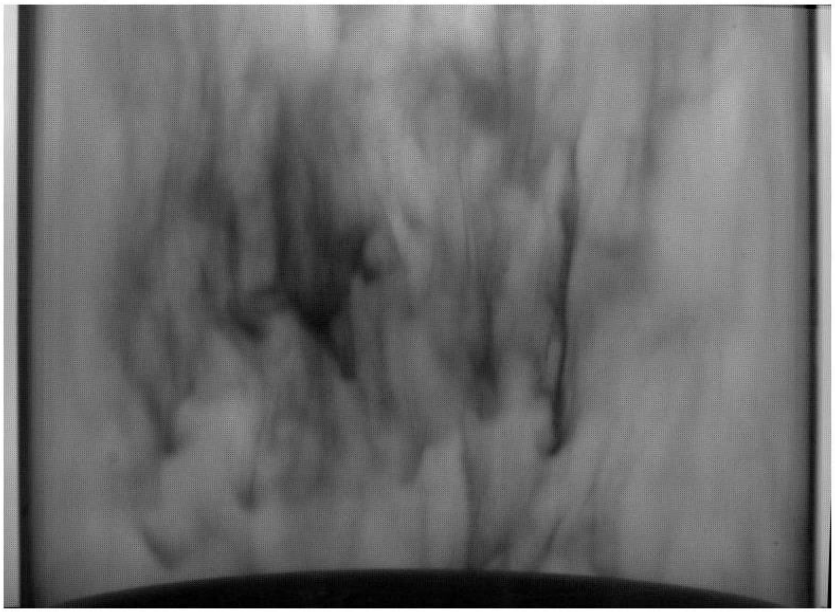

Figure 3-4. Resulting example frame acquired during testing. The falling powder can be clearly seen against the backlight.

A lighting issue that was not anticipated arose during early stages of acquiring footage had to be remedied. Due to the AC nature of the power supply for the backlight, flickering occurs and disrupted the footage data. When plotting pixel intensity across time, a consistent frequency is seen that matches 120 Hz. Figure 3-5 depicts the frequency noise at a frame rate of 700 fps.

Since much of the analysis depends on the pixel intensity values in the frame, this issue was critical to solve. One solution is to switch to a DC powered light however, due to lack of access to one this is not possible for this project. Instead, the frame rate, the number of frames taken per second, is matched to the AC powered light's frequency of 120 Hz to avoid the flickering. Therefore, the frame rate in all the test footage for this research is taken at 120 fps.

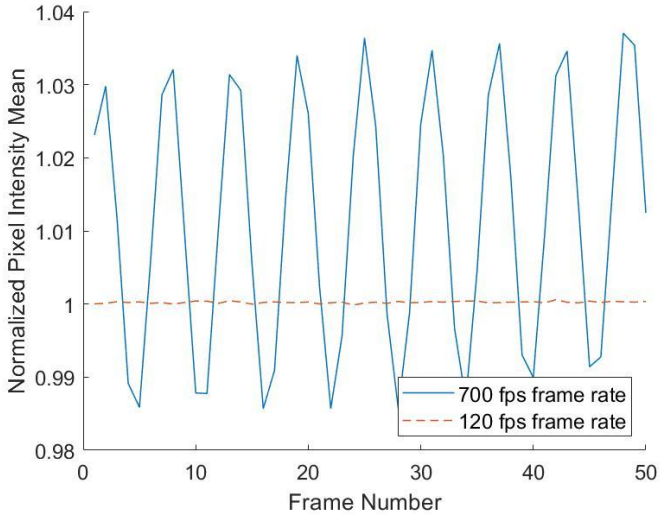


Figure 3-5. Normalized pixel intensity plotted across 50 frames to show the effect of AC lighting. The solid blue line uses footage taken at 700 fps which shows the flickering frequency effects. The dashed orange line uses footage taken at 120 fps with the same light, but the frequency issue is solved.

### 3.1.3 Material

The material used in this study is Tungsten metal powder. The high density of this material is a notable property since this greatly impacts the cloud formations that can be acquired. Dense powders like tungsten will be tested for powder distribution in the future at LLNL, so tungsten is chosen for this thesis for image analysis development. Details on relevant properties of the tungsten powder used in this study are found in Table 3-1.

Table 3-1. Tungsten powder relevant properties.

| | |
|---|---|
| Percent by weight | > 99.7% |
| Mean diameter | 38 μm |
| Density | 19.3 g/cm$^3$ |
| Appearance | Gray to black powder |

### 3.1.4 Safety Considerations

Tungsten metal powder requires certain handling procedures to ensure safe operation. A test procedure with safety guidelines was developed based on material information provided by LLNL and can be seen in Appendix C. This document was approved by Environmental Health and Safety (EH&S) at Cal Poly. Some of the procedures for testing includes wearing face masks and gloves and opening laboratory doors for ventilation while handling the powder. Storage, cleaning, and waste procedures are outlined in the document as well as risk mitigation techniques while powder handling.

## 3.2 Image Analysis

Image processing is the method used to determine the effectiveness of the dust cloud dispersion. The images acquired in the experiment described in Section 3.1 are preprocessed and the distribution of dust in these images is analyzed. The two important aspects to this analysis are spatial distribution of the dust within individual frames as well as how this distribution changes over time. This temporal component to the image analysis requires subsequent frames to be compared to one another so that trends and changes in dust distribution can be observed.

A MATLAB program is developed to preprocess and then fully process the frames to determine the spatial distribution of the powder clouds and how they change with time. A goal of the image analysis program is to use pixel intensity changes to extract a quantitative assessment of the distribution. Additionally, the program is to be able to identify the frame number and resulting time period that has the most uniform dust cloud relative to all the other frames within the footage given a set of parameters. This ultimately could aid in the determination of ignition time for a dust explosivity test application.

### 3.2.1 Dust Presence Through Pixel Intensity

The information for each pixel in a grayscale digital image is a single value of light intensity from 0-255. This intensity value represents the brightness of the pixel which, for this application, can characterize dust presence in that pixel.

The tungsten metal powder used to make the dust clouds in the footage is a dark gray color. Additionally, as mentioned in 3.1.2, a backlighting setup is used when acquiring the footage, so the dust particles block light to the camera and create a strong contrast for where there is dust present in the frame versus no dust presence.

An example of a grayscale image and its corresponding pixel values can be seen in Figure 3-6, where dark pixels have lower intensity values and lighter pixels, nearing white, have values in the higher range, closer to 255. It can then be concluded that dark, light-blocking dust in part of an image will have corresponding pixel intensities lower than those areas in the image that have little to no dust present.

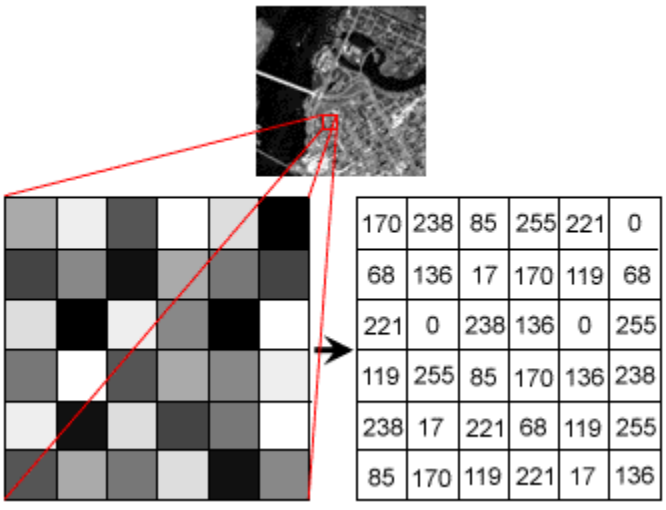


Figure 3-6. Grayscale pixel intensity matrix values shown for part of an example image [13].

### 3.2.2 Preprocessing Steps

Preprocessing steps are employed to make the program more resilient against camera noise and to adjust for variations in image acquisition framing. The first step is to rotate and crop the image in a consistent manner no matter the variations when acquiring the footage. The image is adjusted in this way so that the enclosure walls are vertical, and they are at the edges of the frame. Any space above or below the enclosure is also cropped out to ensure the enclosure makes up the entire frame.

The second preprocessing step is to apply a Gaussian filter to eliminate noise in the raw images. Noise occurs in images for a multitude of reasons including low exposure and a camera's sensor performance. The raw images produced from the high-speed camera have noticeable noise and through tests of different filtering techniques, a Gaussian filter has been determined to reduce the noise in the images, essentially by smoothing the image. A MATLAB function is used to apply the Gaussian function on each image.

The last preprocessing step is a critical one and involves normalizing the pixel intensities in the frames to account for the initial intensities before dust was released. The pixel intensities necessary for the analysis in this thesis should only represent the intensities caused by the dust particles and nothing else. This requires normalization which is discussed in greater detail in the sections below.

### 3.2.3 Normalization by Division

Since this analysis depends on the assumption that the pixel intensities correspond to dust presence, it is important that only intensity changes due to the dark powder is considered. Before any tungsten powder is dropped into the enclosure, there are still pixel intensity values that correspond to unevenness of the backlight distribution as well as general background pixel

values. This initial frame, which can be seen in Figure 3-7, is used in every normalization technique tested to reference all future frames with it.

The first normalization technique implemented is normalization by division where every pixel within a frame is divided by the initial frame's corresponding pixel. This results in normalized average intensity values between 0 and 1. A value of 1 corresponds to no change in intensity therefore no dust present, whereas the closer a value gets to 0 the darker that pixel has gotten due to a large amount of dust present. A resulting normalized frame using this technique can be seen compared to the original frame in Figure 3-8.

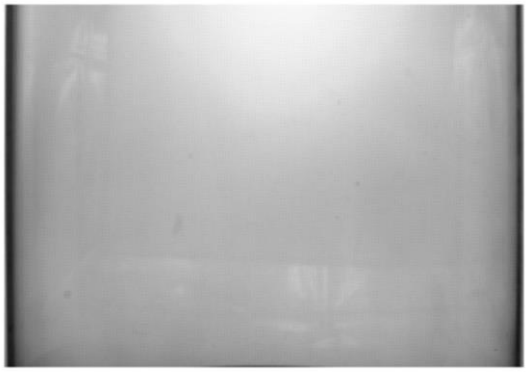

Figure 3-7. Initial frame used in the normalization preprocessing step. The deviation in backlighting can be observed to show a strong hotspot in the upper portion of the frame.

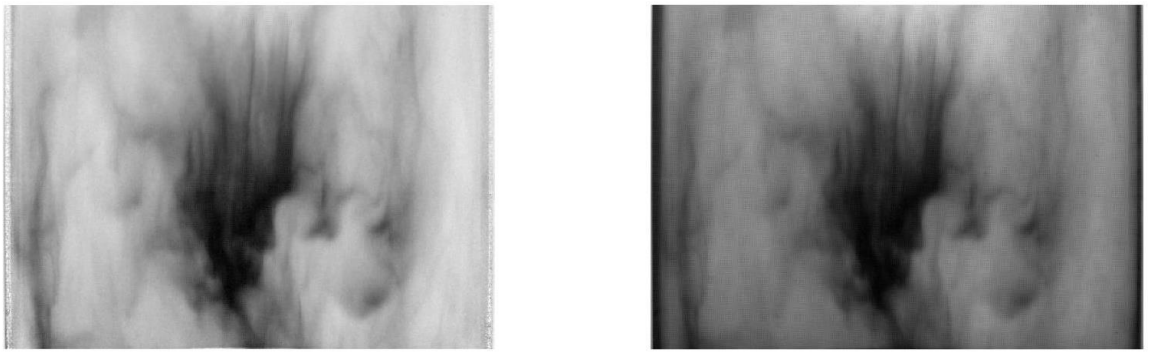

Figure 3-8. Normalized frame by division method (left) and original frame (right). It can be observed that unevenness in the background lighting of the original image is not seen in the normalized image. The normalized image values are displayed in an image viewer in MATLAB where the closer a value is to zero, the darker the pixel is depicted.

### 3.2.4 Normalization by Background Subtraction

An alternate normalization technique that is implemented is to subtract the initial frame pixel intensities from all frames being analyzed. This way, all pixel values being used are the difference between the initial frame and the current frame which should solely be due to powder presence. In order to do this, the initial and current frame matrices are rescaled to be between 0 and 1 and the output after subtraction was between -1 and 0. A value of zero in this case corresponds to no change between the frame pixel and the initial frame pixel, therefore no dust is present. As the value decreases closer to -1, more dust is assumed to be present in that corresponding pixel.

Qualitatively, this normalization technique is similar to the division method stated in Section 3.2.3 in that it keeps the initial intensity values from affecting the values assumed to only represent intensity caused by dust presence. However, both methods are applied and compared to determine the best normalization technique. A resulting normalized frame using this technique can be seen compared to the original frame in Figure 3-9.

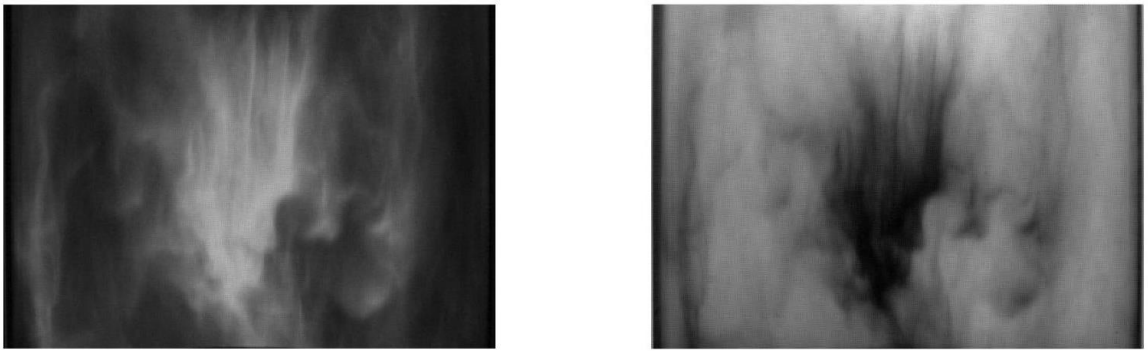

Figure 3-9.Normalized frame by subtraction method (left) and original frame (right). MATLAB depicts values lower than zero as lighter pixels compared to those closer to zero. This is the reason for the inverted image.

### 3.2.5 Normalization by Bouguer-Beer-Lambert Law

An important aspect to note about the previous two normalization techniques is that they do not account for the geometric change in the space that the powder can occupy throughout the cylinder's cross section. This next normalization technique uses the theory of light attenuation through dust clouds to develop a more robust analysis that considers the spatial geometry that the cloud can take up.

In other studies, optical density probes are used to investigate dust dispersion in clouds. These studies use the Bouguer-Beer-Lambert Law which gives the transmission of a monodisperse dust cloud [7] and is expressed as follows:

$$T = \frac{I}{I_o} = \exp(-\beta l) \,,$$

where $T$ is the light transmission, which equals the ratio of transmitted light intensity, $I$, to the incident light intensity, $I_o$. The extinction coefficient, $\beta$, is a combination of the projected area of a powder particle, the number of particles per unit volume, and a dimensionless extinction efficiency factor (not to be confused with the extinction coefficient, $\beta$, which is a different variable) [14]. Additionally, $l$ is the light path length, which is the focus of inclusion in this technique.

Applying this theoretical model includes some assumptions that are not fully met with this application, namely that the cloud is monodisperse and uniform with a monochromatic light source. Although the clouds generated in this study are not monodisperse, as long as the values measured using BBL Law, in this case, $\beta$, are assumed to be an average $\beta$ across the pathlength, the polydisperse cloud is recognized [7]. Additionally, the fluorescent backlight used in this study is polychromatic, not monochromatic. However, past research has been done that applied Bouguer-Beer-Lambert Law using polychromatic light. A key example of this that has been referenced in this research was a study by Zhao and Ambrose from Purdue University, where ambient light was used in a method for sensing suspended dust concentration [12]. Finally,

regarding the uniformity assumption, there is sufficient precedent to still apply BBL in applications with nonuniformity. However, the degree of nonuniformity in this experiment introduces a limitation of this study and a potential source of error.

Using this version of the Bouguer-Beer-Lambert Law, the transmission and the path length is determined and the extinction coefficient, $\beta$, solved for each pixel location. The light transmission, as stated above, is the ratio of transmitted light intensity to the incident light intensity. In this application, transmitted light intensity is assumed to be consistently related to the pixel light intensity from the acquired frames. Therefore, the light transmission is the ratio of the pixel intensity to the initial pixel intensity with no dust present. This is what was solved for in the normalization by division method in Section 3.2.3.

The path length is the distance over which the light transmits through the medium. For this application, the path length is the cross-sectional distance of the cylindrical enclosure, which varies horizontally from the wall towards the center of the cylinder. The path length stays the same at a point moving vertically due to the cylindrical geometry as well as being symmetrical across the vertical axis of the enclosure. A cross-sectional schematic showing the changing path length can be seen in Figure 3-10. A path length matrix is developed to represent the specific path length, in centimeters, of each pixel location of the acquired frames which can be visualized in Figure 3-11. This matrix is used in the calculation of $\beta$ by dividing each normalized pixel value by its corresponding path length. The complete details of how the matrix was generated and $\beta$ solved for each pixel in the frames can be examined in the MATLAB code in Appendix D.

This extra component in this method normalizes not only the pixel intensities with the initial intensities, but also the fact that each pixel represents a path length that the light must travel through the dust cloud for transmission. The resulting $\beta$ values represent the fractional loss of light intensity per unit length through the dust cloud. A resulting frame showing the $\beta$ values for each pixel can be seen in Figure 3-12. This preprocessing method is compared with the results

from the other normalization methods to determine the best technique for processing the pixel intensities to achieve the most accurate cloud distribution results.

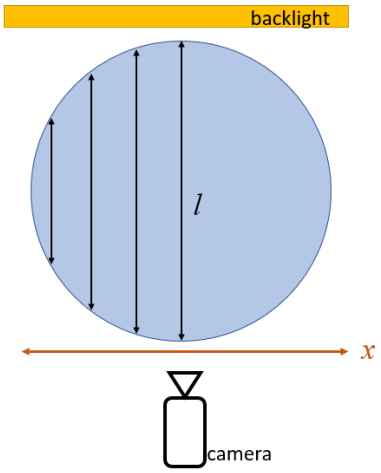


Figure 3-10. Schematic of a top view of the cylinder enclosure showing how the path length, *l*, changes as you move along the x axis which changes how much space the dust cloud can occupy at a given x.

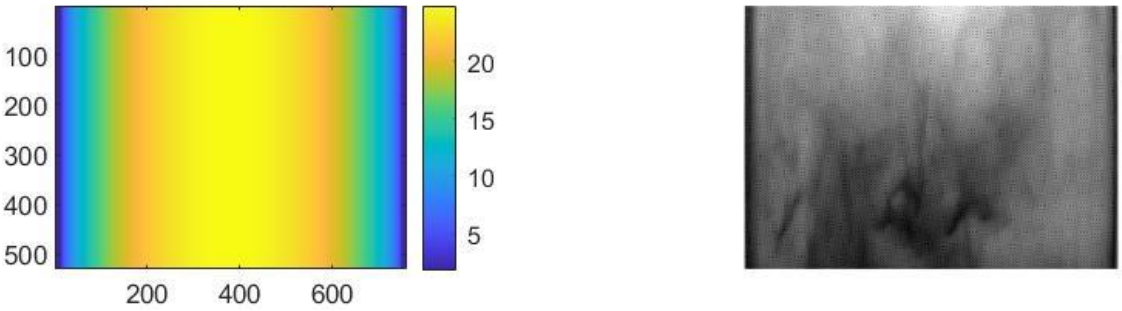


Figure 3-11. Path length matrix displayed with scaled colors representing the length in cm (left) and an example frame which the matrix would be divided from.

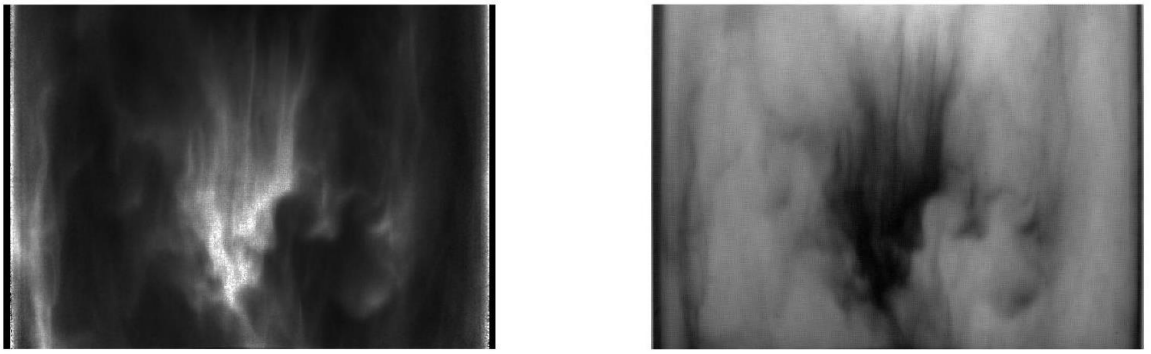

Figure 3-12. BBL law normalized $\beta$ values of each pixel (left) and the original frame (right). The $\beta$ values, which are relatively small in magnitude, are artificially amplified for visualization purposes. MATLAB depicts values lower than zero as lighter pixels compared to those closer to zero.

### 3.2.6 Region Analysis

The main image analysis method used to determine the distribution of the dust in the cloud as it changed with time is region analysis. This is where regions within the enclosure, that represent the entirety of the enclosure, are chosen and relative intensities are measured. This approach allows for visualization of the cloud distribution spatially by quantifying the intensities at different sections of the enclosure. Comparing these regions intensity values measures the uniformity and analyzing this change in uniformity over time assesses the temporal stability of the cloud.

The regions divide the interior area of the enclosure and can be seen in detail in Figure 3-13. The regions are all the same size of 220 pixels wide and 170 pixels high. They are chosen to comprise most of the area that the dust cloud can take up. The sidewalls of the enclosure are not included due to distortion of the high curvature of the enclosure in this area and the lack of dust that occupies it.

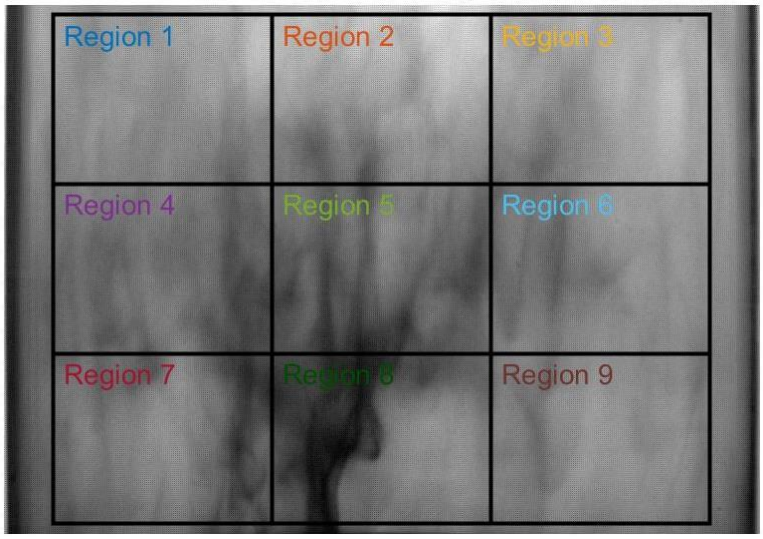


Figure 3-13. Regions that section up the enclosure area that the dust cloud can inhibit. This region scheme is used in analysis to determine the intensity differences and therefore the distribution of the dust cloud through time.

It is important to know where dust is present in the enclosure and where is it not. To analyze this, the sample mean is determined for each region using the normalized pixel intensities within its area. This is done using a MATLAB function to use all the pixel values in a region and output the mean. A plot is then generated where each of the regions' sample mean of normalized intensities are overlayed so that the dust distribution can be understood as it changes with time throughout the footage.

For a uniform dust cloud, there should be little to no deviations between the normalized pixel intensities across the enclosure. In order to quantitatively characterize the variation across areas in the enclosure, the sample standard deviation between the region mean normalized intensities is also calculated at each frame in the footage using MATLAB functions. This is plotted as well to see how the variation of the dust cloud across the enclosure changes with time.

Another important characteristic to determining an optimized dust cloud within footage, especially for the application of determining ignition time during dust explosivity testing, is the stability of the cloud. During ignition time, it is important that the dust cloud is fairly uniform,

but also that it is not rapidly changing in uniformity. Therefore, another measurement calculated from the image data is the average rate of change of the sample standard deviation between the regions. This is calculated by using the sample standard deviation values of adjacent frames. The average rate of change of the standard deviation at a specific frame, *i*, is calculated using,

$$RoC_{SD}(i) = \frac{|SD_{i+1} - SD_{i-1}|}{2}$$

where $SD_{i-1}$ is the standard deviation value at the previous frame, $SD_{i+1}$ is the standard deviation value at the following frame. The change in those standard deviations is divided by the change in frames, which in this case is 2. The absolute value of the difference is used because the direction of the rate of change did not matter for this application. Additionally, the rate of change across only two frames is used due to the relatively slow frame rate of 120 fps that is applied in acquiring the footage. Taking the rate of change across two frames is about 16.7 msec which is a reasonable time frame to access stability of a falling cloud.

### 3.2.7 Alternate Options for Regions

Many variations of chosen regions can be used in the methodology. A couple of these variations have been tested, including smaller areas (150x100 pixels) spread out around the enclosure. This alternate region scheme can be seen in Figure 3-14 and the results from using it in the analysis are compared to the region analysis using larger regions from Figure 3-13. The comparison results, shown in Figure 3-15, reveal that the smaller regions represent the entire enclosure area well; however, there are slight differences in magnitude of both the mean intensity and the standard deviation of the intensities at the frames with the largest dust presence. The larger regions are used in most of the results of this study, however, smaller regions can be used in future applications.


Figure 3-14. Alternate region scheme tested and compared in analysis.

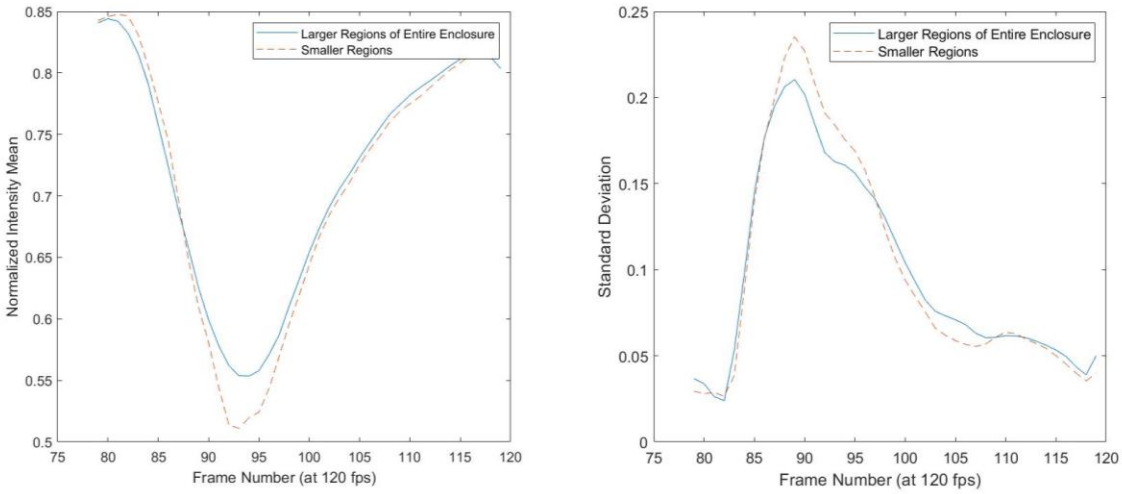


Figure 3-15. Mean normalized intensity in regions (left) and standard deviation between regions (right) versus frame number. The solid blue line represents the data from the large, enclosure-encompassing regions and the orange dotted line represents the data from the smaller regions. The similar results show that using both region schemes are acceptable in application.

For the future application of this analysis on a transparent dust explosion test chamber replica, it is important to have a level of customizability for this region analysis. Certain regions in the chamber are of more importance to have uniformity, like the center area around the

ignitors. Due to this need, the region analysis is customizable by the user to include whatever regions they may want to analyze. Regardless of the chosen regions, the analysis algorithm performs the same in determining the normalized intensities, relative sample means of the region intensities, sample standard deviation between these region intensities, and the rate of change of the deviation.

Additionally, optical density probe studies are a common method of analyzing density concentration and distribution of dust clouds as mentioned previously. Comparing results from optical density probe measurements and corresponding high-speed camera pixel intensity results has been done by Zhao et al. [12] and similar applications may be done using this methodology. In order to do this, the region chosen in the frame could follow where the laser or light source crosses to take intensity measurements. An example region for this application can be seen in Figure 3-16. A 'radial trace', or a defined region horizontally across the enclosure that follows a light source to an optical probe, can be used to acquire intensity data. This data would need to utilize the Bouguer-Beer-Lambert law processing from Section 3.2.5 to output an extinction coefficient value from the transmission intensity and path length components. This application is explored in more detail by Grenley [15].

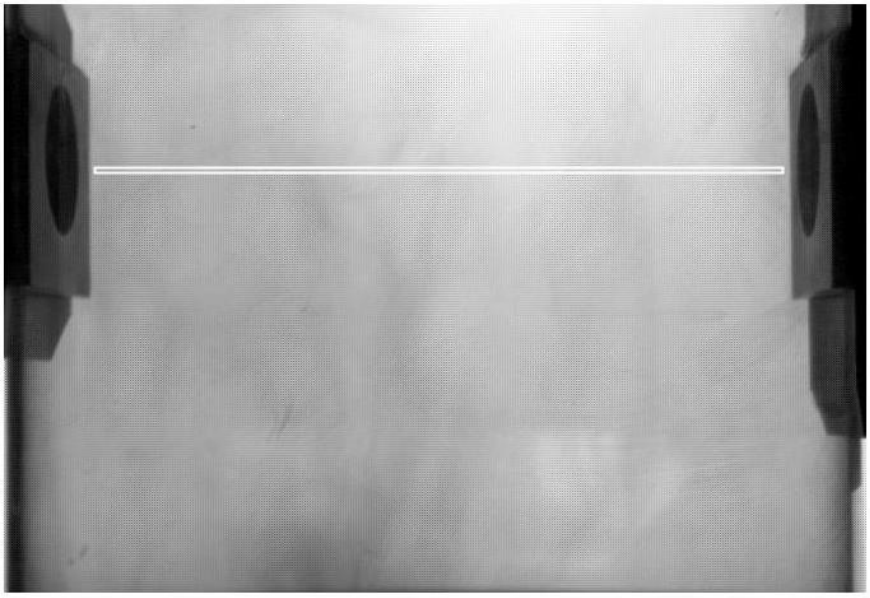

Figure 3-16. Laser trace region to be potentially applied for comparing optical probe dust cloud measurements to image analysis measurements.

### 3.2.8 Criteria Application to Determine Point of Greatest Uniformity

As previously mentioned, a goal of the image analysis from this study is to be able to identify the point of greatest uniformity of the dust cloud relative to the other frames within a given high-speed video. The region analysis generates important measurements from the dust cloud in all the frames including sample mean intensities, sample standard deviations, and rate of change of the sample standard deviations. However, this data can be analyzed and optimized to find points at which there is a uniform and stable powder cloud present. In order to do this, criteria are developed to evaluate the hundreds of frames within each video.

For each frame, the regions' mean intensity values are averaged with each other to output a single sample mean intensity for each frame. This mean intensity is representative of how much dust is present in the enclosure at that frame. The first criterion applied to the measurement data is a threshold for this mean intensity value to ensure that, in fact, there is a dust cloud present in the frame, and it includes enough dust for a certain application. In application, this threshold could take the form of a straight intensity value cutoff from the range of values that exists in a video, or

it could be determined be a percentile of the intensity values. If a straight threshold value is determined, rather than by using a percentile, then this does pose a risk that none of frames will satisfy this criterion and no output is determined. In order to avoid this, in this study, a percentile is used to determine the intensity threshold using a percentile MATAB function. Applying a $20^{th}$ percentile threshold on the normalized intensity data calculates the $20^{th}$ percentile of that specific intensity data set, which can change footage to footage, and every frame that has an intensity value lower than that $20^{th}$ percentile value, satisfies the criteria. Any frame with a mean intensity above that value does not have enough dust present and is eliminated from the data set for being chosen as an optimized frame.

The next criterion applied to the remaining frame data ensures the stability of the cloud at that time and that it is not rapidly changing in uniformity. A threshold is developed for the rate of change of the standard deviation. This study uses a percentile of the rate of change data to determine the threshold. Again, the type of threshold depends on the specific application. By applying this threshold, frames with a standard deviation rate of change below this threshold, indicating greater temporal stability, satisfies this criterion.

The final criterion applied to the frame data is regarding uniformity. As previously mentioned, for a perfectly uniform dust cloud, there should be little to no deviations in the pixel intensities across the enclosure. Therefore, the most uniform point of the dust cloud occurs when the standard deviation between the region intensities is the smallest. Using the remaining frame data that have already satisfied the previous two criteria, an output frame is determined by finding the frame with the minimum sample standard deviation. This ensures that, if any frames already satisfied the previous two criteria, the program outputs the most uniform cloud that exists in those frames. More than one frame can be output by this process by finding multiple frames with the lowest standard deviation. In this study, this minimization technique is applied to determine three frame numbers at which the criteria are satisfied in the footage.

An alternative way this uniformity criteria can be used is through applying a specific threshold value on the standard deviation data which would ensure a sufficient uniformity based on the input. This, however, does not guarantee that an output will result. In the case where none of the remaining frames are below the standard deviation threshold, the cloud never reaches the level of uniformity, dust presence, and stability required based on the parameters. This alternative method is not used in the analysis of this study.

The output frame(s) from applying criteria helps sift through all the results from the region analysis for the determination of a desired dust cloud time frame. This may have the potential for application in determining the ignition time for a dust explosivity test. Additionally, this also may be a useful check in determining if a dust cloud distribution ever even reaches a desired uniformity with necessary concentration or stability requirements.

# 4 RESULTS AND DISCUSSION

## 4.1 Dust Distribution by Region Results

When applying region analysis on the footage data, the region intensity plots show a very cyclic cloud at the same frequency of the motor that tapped the sieve in the testing apparatus, which is to be expected. A dust cloud coming into frame is represented by a downward peak in intensity, which is seen in Figure 4-1. Four falling clouds can be observed in the figure with trends in the normalized intensity of certain regions in all dust clouds. A more comprehensive visual assessment on a single cloud is detailed further in this section.

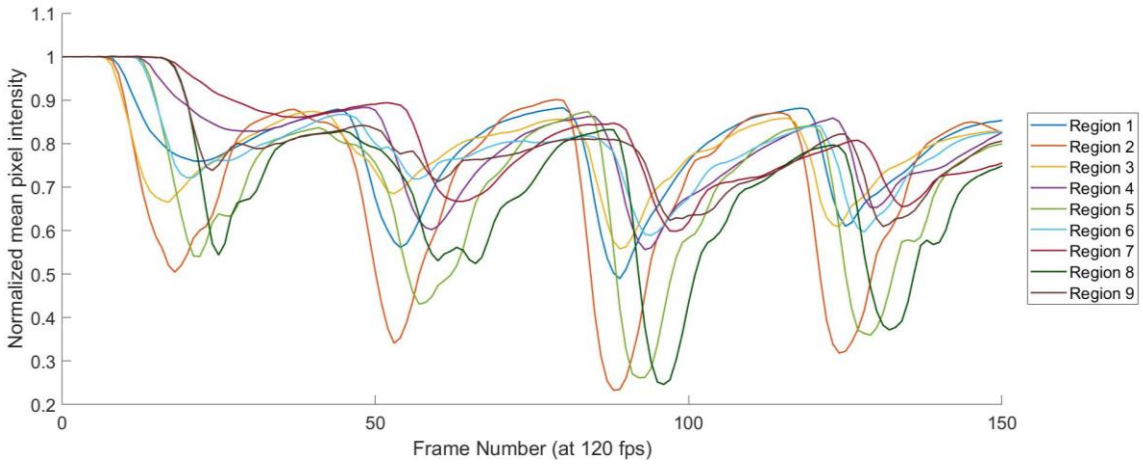


Figure 4-1. Region mean intensity normalized by division as it changes temporally across 4 falling dust clouds. Before any dust enters the frame, all regions have a value of 1, however when dust entered each region, their normalized intensities lowered to values corresponding to the amount of dust present.

Figure 4-2 compares the different preprocessing normalization techniques used on the intensity data for the same dust cloud. The results show a very similar behavior of the data regardless of preprocessing method used. With respect to the temporal response of the region mean intensities, the trends between the different methods are the same. Dust enters the frame, specifically in region 1, 2, and 3 at a little before frame 10 in all three plots, and subsequently enters regions 4, 5, and 6 and then 7, 8, and 9 before frame 20. The temporal progression is very consistent in all methods being compared.

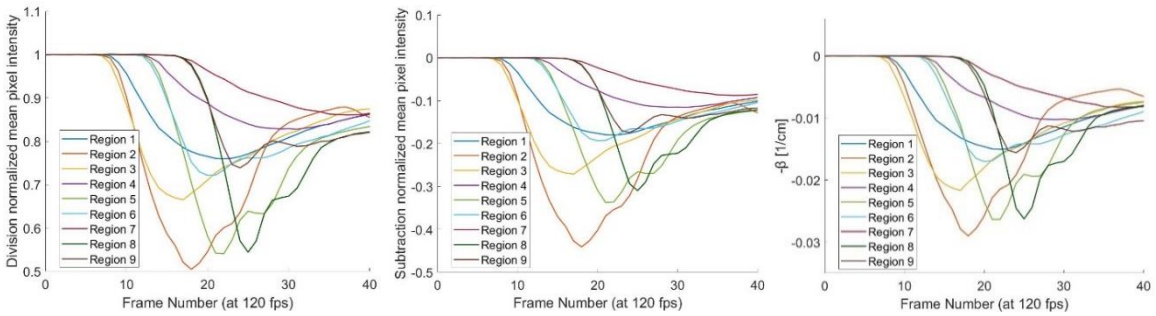


a) b) c)

Figure 4-2. Region analysis results from a single falling cloud using a) normalization by division of initial frame b) normalization by subtraction of initial frame, and c) normalization by BBL law.

Due to the different preprocessing methods, the normalized intensity y-axis on the plots of Figure 4-2 cannot be directly compared. The scales for the division normalization and subtraction normalization are 0 to 1 and -1 to 0, respectively. The path length normalization method solved for -β, which has units of 1/cm and has a much smaller, logarithmic scale due to the nature of Bouguer-Beer-Lambert Law. The value of -β is plotted instead of positive β to be consistent with lower intensity values indicating more dust presence as previously discussed in 3.2.1. Although the magnitudes of the plots cannot be compared between one another, the relational magnitudes between the regions within each individual plot are observed and compared.

In this regard, it is observed that the intensity magnitude of the center regions, 2, 5, and 8, are lower relative to the magnitudes of the other regions in all three of the intensity plots. This suggests that more dust is present in the center of the enclosure than the sides for this cloud and this is identified by all preprocessing methods. The general trends of the relative magnitudes for all three techniques are very similar to one another with some subtle differences. An interesting difference between plot a) and plot b) in Figure 4-2 is that all three center regions at their minimum are similar in magnitude with one another in plot a) but the relative minimum magnitudes are different in plot b). In plot b), region 2, in orange, has a lower magnitude than the

other two center regions at their minimum. This may be a function of the increased mathematical sensitivity of the subtraction method to different initial background intensities when there is a large difference between the frame pixel intensity and the initial pixel intensity. The initial background frame in Figure 3-7, reveals a bright hotspot at the top of the frame from the backlight equipment. This bright hotspot is in region 2 and is suspected to have contributed to the subtraction normalization sensitivity differences observed in Figure 4-2. This also illustrates a limitation with this normalization method in how it is affected by inconsistent backlighting.

Additionally, when comparing the division normalized intensity plot a) to the -β plot c), it is observed in plot a) that the center regions' magnitudes are very low with respect to the other regions. However, for the -β intensity plot c), the center regions' magnitude relative to the other regions reveals a much smaller disparity. This makes sense for the disparity between the center regions to the other regions to be smaller in plot c) because the intensity ratio values were ultimately divided by the largest path length values in the center, resulting in smaller magnitudes relative to the edge regions.

For the remainder of the section, only the BBL law normalization technique results will be presented and discussed. This technique is decided to be the most robust method to preprocess the pixel intensities due to the inclusion of the governing attenuating light theory. Relating the pixel light intensities to an extinction coefficient, β, is a more physically legitimate measurement for dust presence. In addition to this theoretical reasoning, as is seen above in Figure 4-2, the results of the normalized intensities compared to -β are very comparable, not in scale, but in relative magnitude and temporal behavior. All aspects of the region analysis, including applying statistical criteria, has been performed on all the footage three times, using the different techniques. The results show very few differences between the methods. Therefore, due to this consistency and the physical robustness mentioned above, -β is assumed to represent the intensity due to dust presence in the frames for the remainder of the study.

Looking closely at one falling dust cloud, a visual verification of the image analysis results using this method is achieved. Figure 4-3 shows three frames, frame 108, 112, and 116, equally spaced through the time a single dust cloud falls in and out of the frame. The -β mean values for each section throughout this dust cloud is observed in Figure 4-4. The -β plot has each of the three frame positions identified with a dashed line.

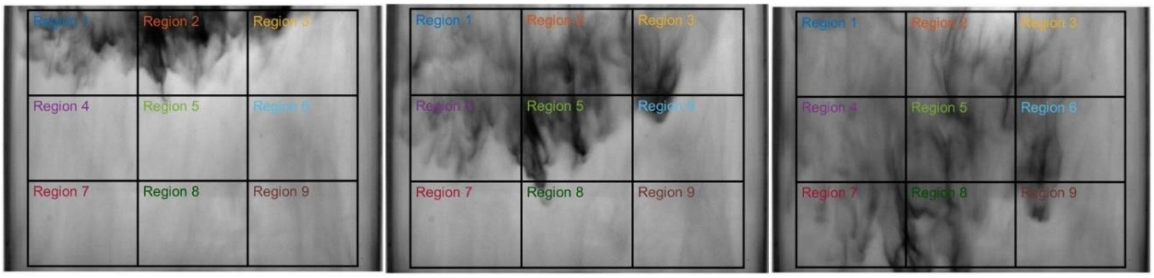


Frame 108 Frame 112 Frame 116

Figure 4-3. Three sequential frames within a single dust cloud from acquired footage. The regions used in the region analysis are overlayed on the images for reference.

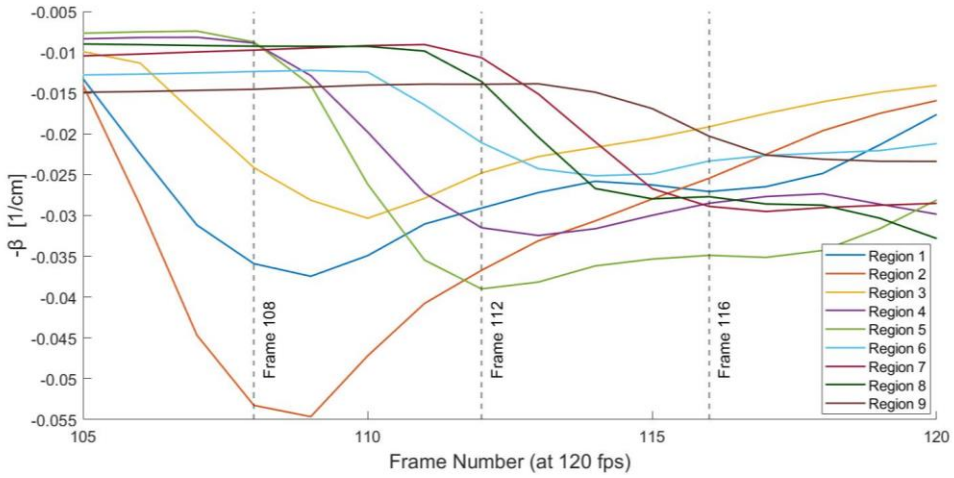


Figure 4-4. -β mean values for each of the regions throughout all frames in a single cloud. Positions for frames 108, 112, and 116 are shown in dashed lines for reference.

Frame 108 shows tungsten powder falling from the top of the frame and that the powder is mostly present in regions 1, 2, and 3. Figure 4-4 validates this with -β values actively lowering

in all three of those regions around frame 108 on the plot while the other 6 regions do not vary much with one another.

Looking at the visual image of frame 112 in Figure 4-3, much of the tungsten powder present has entered regions 4, 5, and 6 with less powder in region 2 than previously in frame 108. When comparing this visual image to the -β information at frame 112, these characteristics of dust presence are depicted in the plot. This can be seen in regions 4, 5, and 6's -β values at frame 112 dropping considerably since frame 108. Additionally, an increase in region 2's -β value from its minimum at frame 108 indicates that there is less dust presence in the region than before.

Finally, looking at the frame 116 image in Figure 4-3, it id observed that the dust is reasonably distributed across the regions, with lightly less dust present in the right regions 3, 6, and 9. This verifies the results from the -β plot at frame 116, where the -β values for all regions were the closest to one another compared to the other discussed frames and that the right regions 3, 6, and 9 all had the lowest -β with respect to the other regions. This consistency shows that the -β values are representative of dust presence in the corresponding regions and frames, as assumed.

The sample standard deviation results of the region analysis across the frames in the same falling dust cloud are displayed in Figure 4-5. It is observed that the -β variance between the regions is highest at frame 108 and lowest at frame 116. As previously discussed, the sample standard deviation between the regions is assumed to describe the uniformity of the dust distribution, where a high standard deviation indicates low distribution uniformity, and a low standard deviation indicates increased distribution uniformity. When comparing the individual frames in Figure 4-3, this is consistent with this assumption. This is seen in examining frame 108 which has very little distribution uniformity across the enclosure and therefore a high standard deviation. Additionally, the most evenly distributed frame of the three, frame 116, shows the lowest standard deviation value.

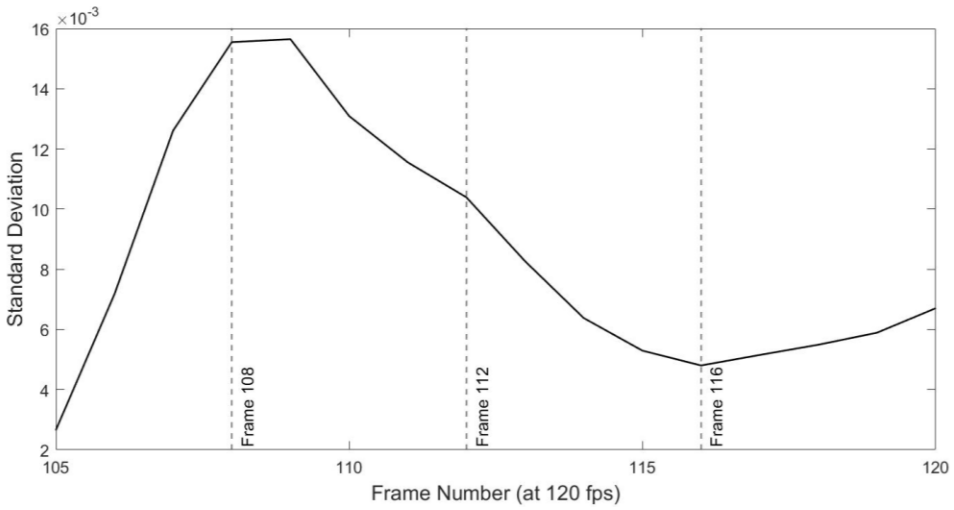


Figure 4-5. Sample standard deviation of the -β values between each of the regions at all frames in a single cloud. Positions for frames 108, 112, and 116 are shown in dashed lines for reference.

The standard deviation rate of change results across the same frames in the single dust cloud discussed above are displayed in Figure 4-6. It is observed that the stability of the dispersion, indicated by the magnitude of the rate of change values, is similar at frame 108 and frame 112. Additionally, frame 116 has a lower standard deviation rate of change value, suggesting the cloud is more stable at that point. Both frames 108 and 112 are at points where the beginning of the dust cloud is actively falling into space not previously occupied by much dust. This inherently causes change in variation of the region intensities from one frame to the next. This results in the rate of change value being higher relative to a point in time where the cloud is dispersed across the enclosure and more dust is continuing to fall to keep the variation minimized, which is seen in frame 116.

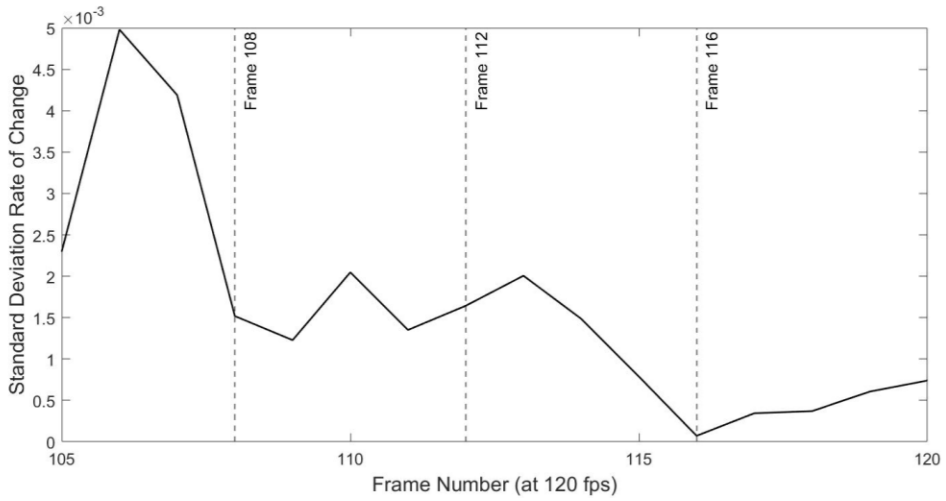


Figure 4-6. Rate of change of the sample standard deviation across immediate adjacent frames for all frames in a single cloud. Positions for frames 108, 112, and 116 are shown in dashed lines for reference.

## 4.2 Statistical Criteria Application Results

Now that the results in which to characterize the distribution of dust have been visually verified, the statistical criteria, discussed in 3.2.8, are applied to these results for each of the frames. This includes applying a -β threshold, a standard deviation rate of change threshold, and then finding three frame numbers where the standard deviation is minimized. The specific thresholds applied are a threshold defined by the 20$^{th}$ percentile of -β data and a threshold defined by the 35$^{th}$ percentile of the standard deviation rate of change data. These thresholds are chosen arbitrarily since this study has no ideal frame number to output from a reference cloud for calibration. However, variations of the input parameters are examined in Section 4.3. As a proof of concept, three frames are output by this analysis to determine the three most optimized frames in the footage for dust presence, cloud uniformity, and cloud stability given the input threshold parameters. The results are seen in Figure 4-7 and Figure 4-8.

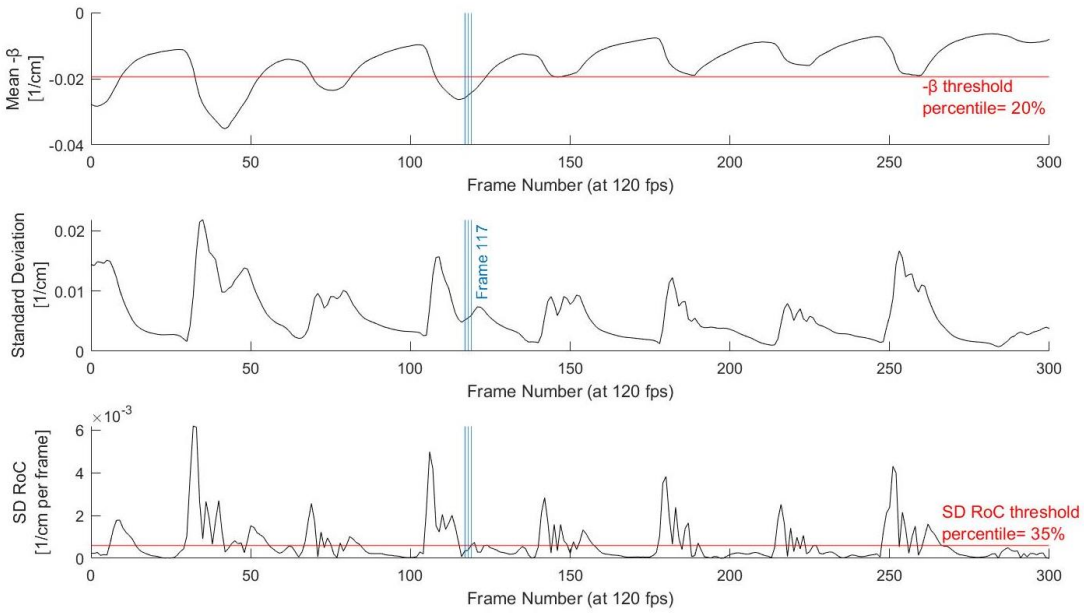


Figure 4-7. Footage 3 analysis results of mean -β, standard deviation, and standard deviation rate of change plots (top to bottom). A 20-percentile -β threshold and a 35-percentile standard deviation rate of change threshold (shown in red) is applied to the results. The three frames optimized for these criteria are output and are shown in blue to be frames 117, 118, and 119.

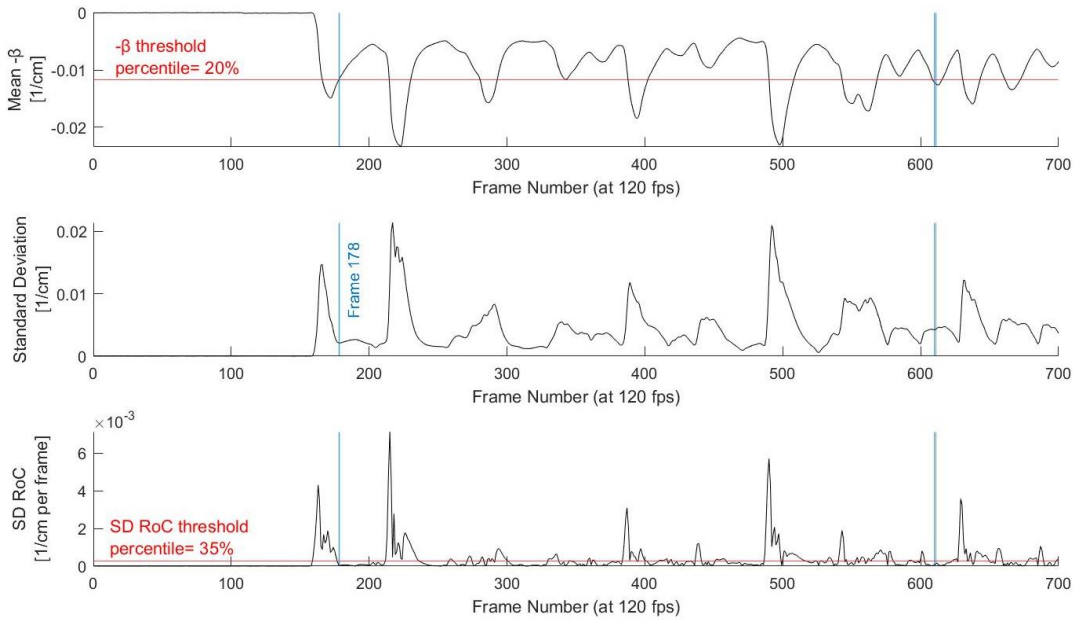


Figure 4-8. Footage 4 analysis results of mean -β, standard deviation, and standard deviation rate of change plots (top to bottom). A 20-percentile -β threshold and a 35-percentile standard deviation rate of change threshold (shown in red) is applied to the results. The three frames optimized for these criteria are output and shown in blue to be split between two points in the footage.

The results above show the output of applying statistical criteria to the data. This is also done with the other footage acquired, 5 videos total, and most, (4/5) of them, output three frames adjacent to one another, like in Figure 4-7. However, the analysis also has the possibility of identifying frames that meet all the criteria and minimize the standard deviation at different clouds in a single footage take. This shows that multiple nonadjacent points can be identified as similar in uniformity depending on the criteria used. This outcome is also a product of the type of dust dispersion used in this study. The dust clouds generated in the footage are cyclic, but unique clouds which occasionally have similar uniformity with one another can be present. With other dust cloud formations for different applications, like in an explosivity testing chamber, the dust is shot up and forms a single falling dust cloud with various stages in development. This alternate dust cloud dispersion likely has a single range of time that possesses the greatest uniformity.

Since the experimental setup for this study generates unique, nonrepeatable clouds that never acquire absolute uniformity, there is no known “best frame” to accurately verify or reference the result output frames. The output frames of greatest uniformity are with respect to the other frames within the footage and depend upon the input threshold parameters.

## 4.3 Parameter Study

As discussed in the section above, the threshold parameters are crucial in determining the desired output for a specific application. It is then important to understand how sensitive the output is with varying parameters. The results of the statistical criterial output are shown as they change with varying threshold parameters.

Specifically, the results are compared with frames that have been visually identified as uniform with respect to the other frames in the video to serve as a reference to whether the program is behaving as expected. These 2-4 frames are identified through manual examination of all frames in the acquired footage for uniformity and dust presence and are referred to as “chosen frames”. This choosing process has a factor of subjectivity, as it is not always obvious what frame has the best uniformity, if any, which is why multiple frames are chosen. These chosen frames are not used as a verification of the program, but more as a reference to what types of frames that the method is outputting given varying parameters.

Since it is not realistic to expect the program to output the exact chosen frames, the distance between the output frame number and the previously chosen frame number is calculated. If this distance is less than 5 frames, the output is assumed to be close enough to be referenced from that chosen frame, since adjacent frames are similar to one another.

The -$\beta$ percentile threshold is varied from 1-30$^{th}$ percentile which changes how much dust presence is needed to satisfy the threshold requirement. Six different standard deviation rate of change thresholds are also tested that ranges from the 20$^{th}$ to the 45$^{th}$ percentile of the rate of change data to observe how the stability criteria affects the output results. The outcome of this

parameter study with the “chosen frames” is seen in Figure 4-9 and Figure 4-11 for footage 3 and footage 4, respectively.

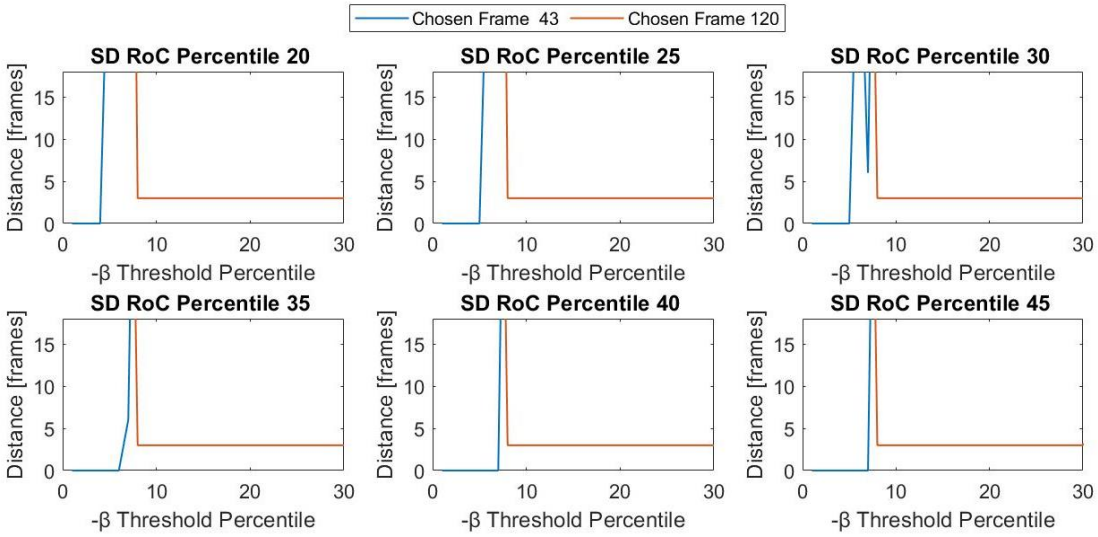


Figure 4-9. Parameter study of footage 3 to see if the visually chosen frames are identified with differing parameters. Each plot depicts the distance of the output frame to the predetermined chosen frames as it varies with an increasing -β threshold percentile. The standard deviation rate of change is different for each of the six plots and the percentile value used to determine the threshold is seen above each plot.

The parameter study performed on footage 3 shows how the frame output is fairly consistent with a $10^{th}$ to $30^{th}$ -β percentile threshold and that it identifies the most uniform frame to be within the 5-frame distance of the chosen frame 120. However, with a -β threshold smaller than the $5^{th}$ percentile, the program identifies another chosen frame, frame 43. During the transition between these two identified frames, there are some inconsistencies for the output frame. This reveals that by changing the -β threshold, the output is altered. Figure 4-10 displays the two frames that are output by applying the different criteria. Frame 43 is shown to have a much heavier dust presence in frame than frame 120, however with less uniformity than frame 120 shows. This is consistent with the results of Figure 4-9, which demonstrates how frame 43 is identified when the -β threshold is lower, requiring more dust presence in the frame. However, at

a less restrictive threshold of approximately the 8$^{th}$ percentile, frame 120 satisfies this criterion and is identified as the frame with the greatest uniformity.

Minimal changes between the plots with the varying standard deviation rate of change thresholds are observed. This reveals that this method is less sensitive to that parameter using this footage's data.

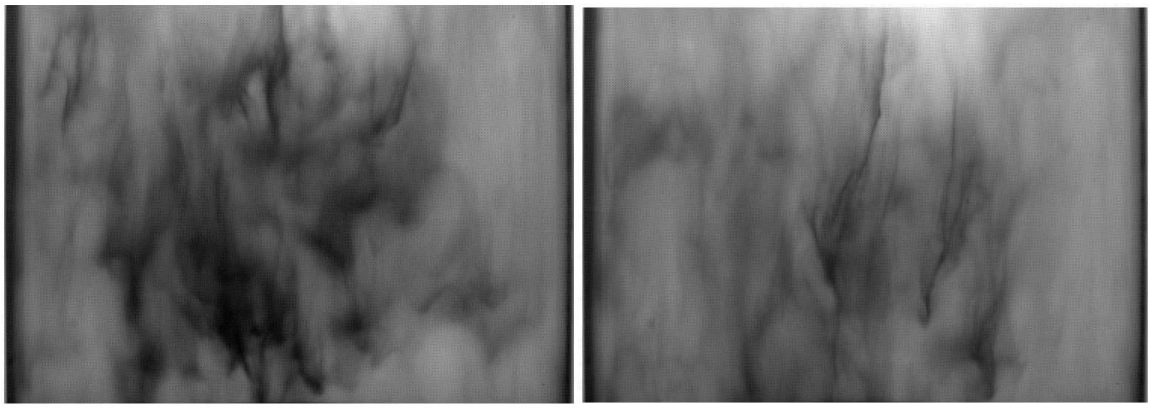

Figure 4-10. Frame 43 (left) and frame 120 (right) in footage 3, which are output as optimum frames depending on the different -β thresholds requiring different intensities of dust presence.

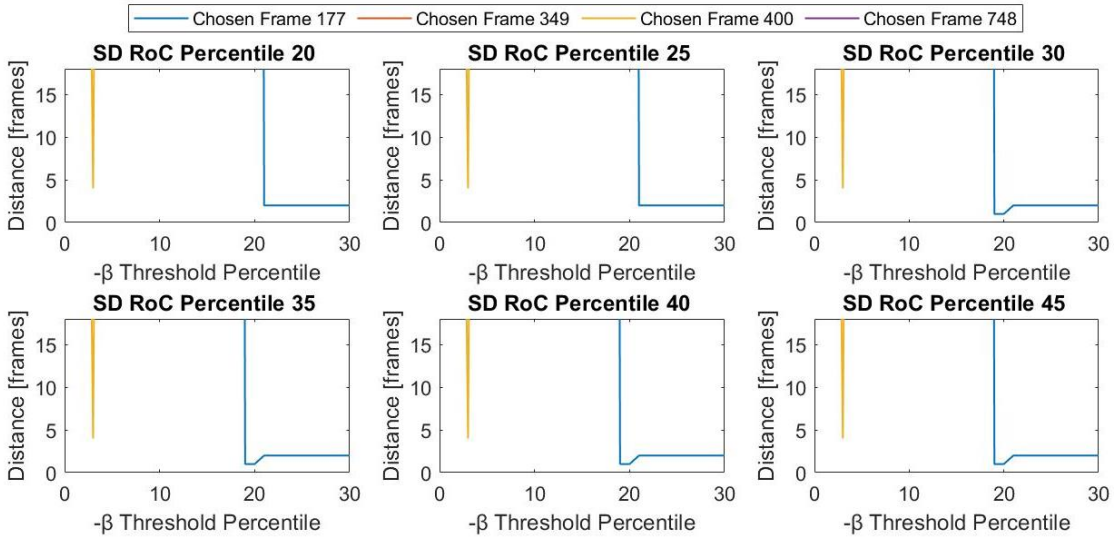


Figure 4-11. Parameter study of footage 4 to see if any of the visually chosen frames are identified with differing parameters. Each plot depicts the distance of the output frame to the predetermined chosen frames as it varies with an increasing -β threshold percentile. The standard deviation rate of change is different for each of the six plots and the percentile value used to determine the threshold is seen above each plot.

The parameter study results for footage 4 show how the frame output is fairly consistent with a -β threshold after about the 20$^{th}$ percentile. At this threshold, the most output optimum frame is identified to be within the 5-frame distance of the chosen frame 177. However, with a -β threshold smaller than the 20$^{th}$ percentile, none of the chosen frames are consistently identified. This reveals that the -β threshold parameter must be above the 20$^{th}$ percentile to identify the amount of dust desired in the chosen frames. Figure 4-12 displays the four frames that had previously been chosen through visual inspection to have the greatest uniformity. By observing the dust distribution in these frames, the dust presence is somewhat similar, but the distribution is more uniform over the entire enclosure for frame 177. These other frames were not identified as the most optimum frame after they satisfied the -β threshold due to their higher sample standard deviation value compared to frame 177.

Similar to the results from footage 3, not much change is observed between the plots with the varying standard deviation rate of change threshold. This again reveals the output method using this footage's data is not very sensitive to the stability parameter.

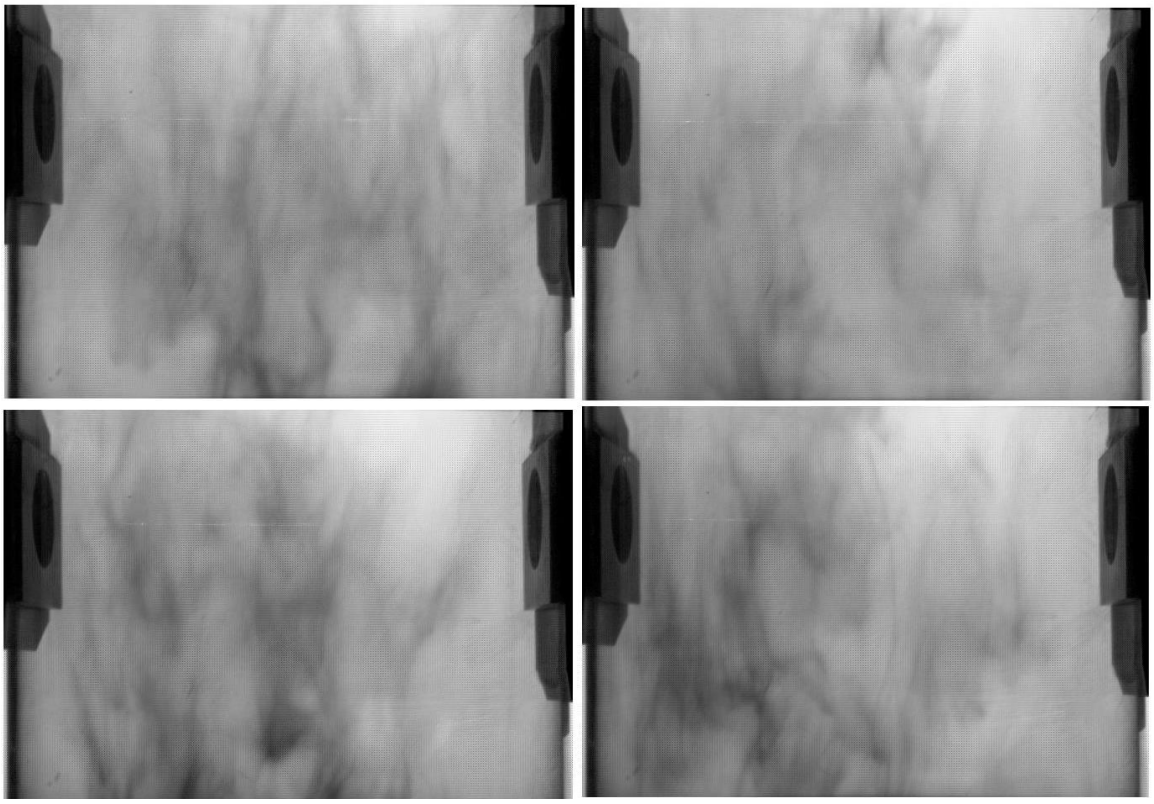

Figure 4-12. Frames 177, 349, 400, and 748 (top left to right, bottom left to right) in footage 4, which were the chosen frames from the preliminary visual identification used to assess the criteria application output.

The parameter study results show that output frame results are much more sensitive to the pixel -β threshold than the stability criteria threshold when processing images generated in this thesis. This method of varying the parameters is useful in understanding the sensitivity of the output given these parameters for a video. Additionally, this parameter study is useful in determining the necessary thresholds if a desired frame is known for a video.

## 4.4 Dust Explosivity Testing Chamber Replica Application

This image analysis process is applied to high-speed footage from LLNL's transparent replica of their modified dust explosivity testing apparatus. The pressurized transparent globe is vacuum sealed and 120 grams of tungsten powder was shot in with a net pressure gradient of 20 bar. This dust dispersion method produces a much different cloud than what is generated experimentally in this study. In LLNL's footage, the powder shoots upward out from the nozzle to form a plume, hits the top of the globe, and then falls back down in the form of a dispersed cloud. The progression of the dust distribution is shown in Figure 4-13.

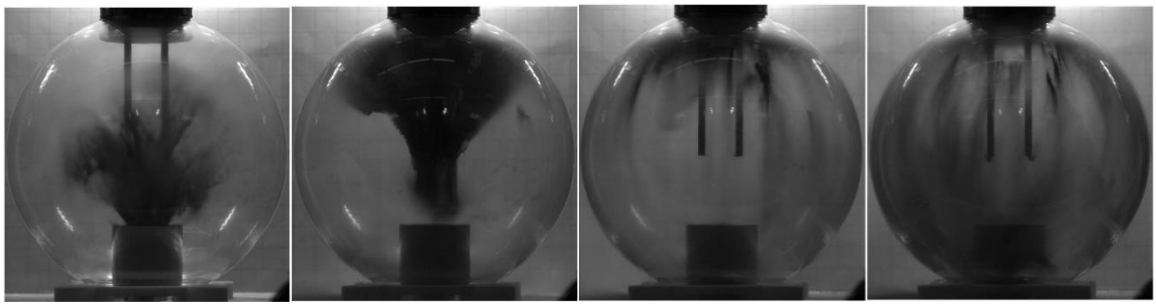

Figure 4-13. LLNL footage dust cloud dispersion progression.

The region analysis is performed on this footage the same as outlined in Section 3.2.6 with a couple minor adaptations. Due to the shape of the enclosure being spherical rather than cylindrical, the path length matrix used to calculate -β, as discussed in Section 3.2.5, is adapted to fit the geometry of the sphere as can be seen in Figure 4-14. Additionally, due to the differing shape and obstructions in the enclosure, smaller regions are used in the region analysis and are seen in Figure 4-15. Obstructions in the enclosure create dead zones and are not representative of the dust presence in that area. As shown previously in Figure 3-15, using smaller regions is still representative of the entire enclosure and the results are very similar to using larger regions that make up the entire enclosure.

Another adaptation to the previously described analysis is in calculating the standard deviation rate of change. More frames are used in calculating the average rate of change due to

the substantially faster frame rate of the LLNL footage, specifically 10000 fps. And finally, the last adaptation to the analysis is to output the 10 most optimized frames rather than 3, to identify a larger time range. The increased frame rate results in smaller changes in between frames which warrant increasing the output frames due to their similarity. The specifics of these changes can be observed in the MATLAB code in Appendix D.

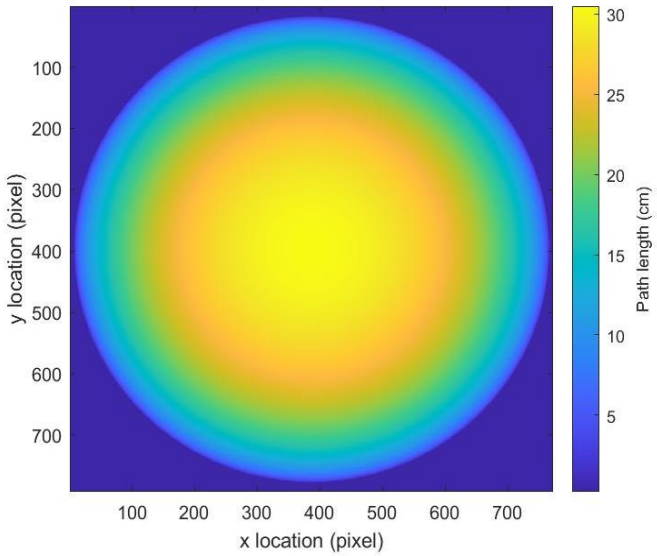


Figure 4-14. Path length matrix for the spherical LLNL test enclosure showing the path length values for each pixel location in centimeters scaled with colors.

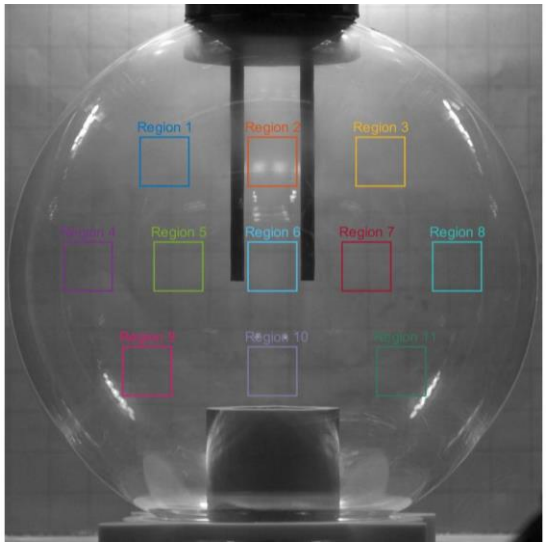


Figure 4-15. Regions used in the image analysis process on LLNL testing apparatus footage. More regions are added to include more of the enclosure, but smaller regions are utilized to avoid obstructions that may have skewed data otherwise.

The image analysis process is applied to the footage and the region analysis -β plot can be observed in Figure 4-16 to show the dust distribution across the globe through regions. Additionally, the results shown in Figure 4-17 display the temporal trends of the distribution dust presence, uniformity, and stability.

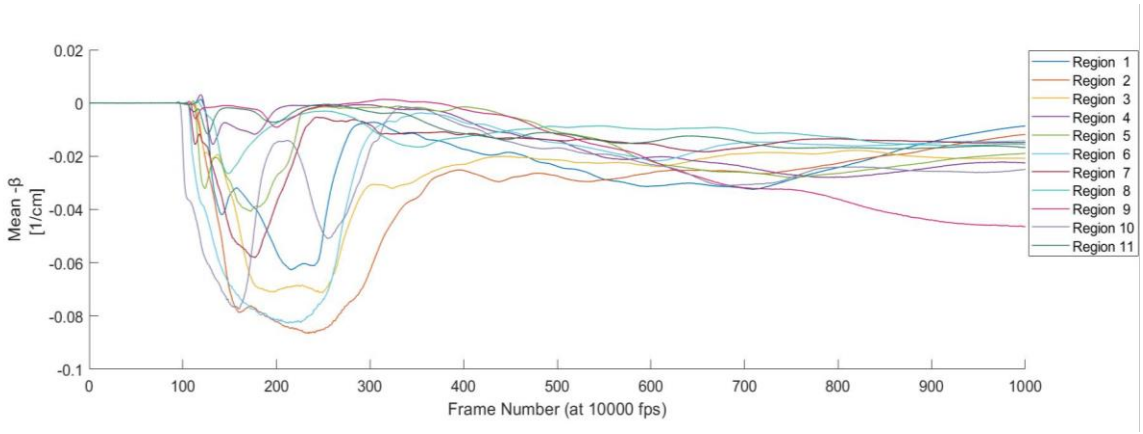


Figure 4-16. LLNL footage analysis results showing the mean -β value for each region to represent the dust presence spatially across the globe at different points in time. This plot shows the initial blast of powder upward from about frame 100 to frame 300. Then the powder begins to fall and the -β values of the regions decline as more dust distributed across the enclosure.

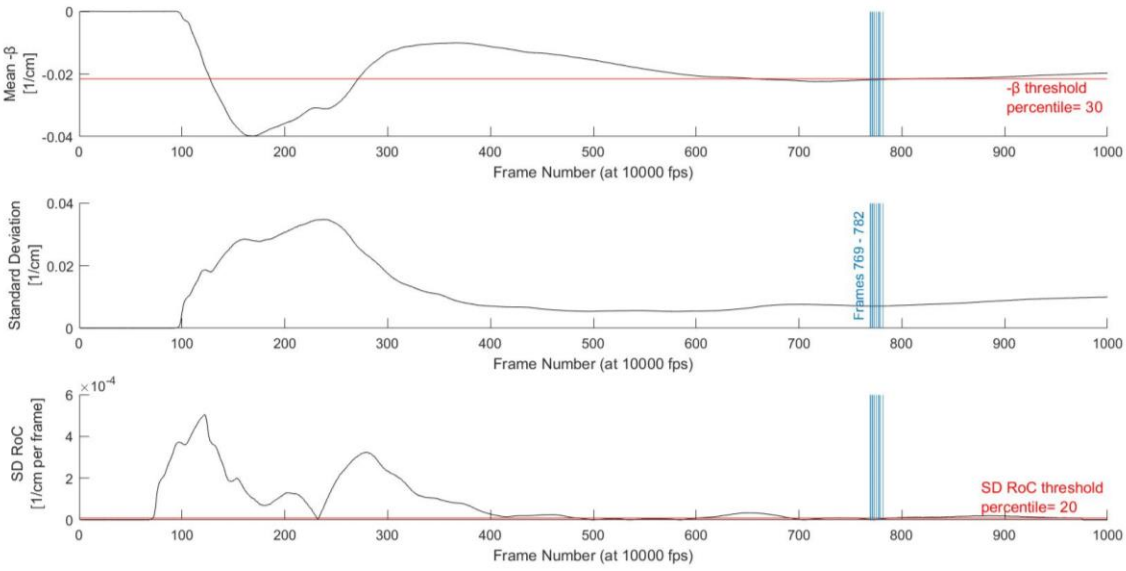


Figure 4-17. LLNL footage analysis results of total mean -β, standard deviation, and standard deviation rate of change plots (top to bottom). A 30-percentile -β threshold and a 20-percentile standard deviation rate of change threshold (shown in red) is applied to the results. Ten frames are output as most optimized for these criteria and are shown in blue to be between frame 769 to 782.

Figure 4-18. Frame 771, one of the resulting output frames from the statistical criteria applied. The other frames output by the analysis are similar in time frame. Due to the very fast frame rate of the footage, the powder distribution in the frames from 769-782 barely changed at all.

As can be seen in the -β plot, the dust shoots up at around frame 100 and the dust presence is very high in that plume, so the -β values are very low. However, at this same point in the standard deviation plot, the values are very high due to the plume being concentrated in one area of the globe. After the dust has rebounded, it begins fall and reenter much of the enclosure in a dispersed manner which is revealed with the mean -β and the standard deviation lowering in magnitude. Additionally, during this period of slower, dispersed particles falling, the standard deviation rate of change is small showing the cloud is relatively stable at those frames.

A $30^{th}$ percentile -β threshold and a $20^{th}$ percentile standard deviation rate of change threshold is applied to the footage analysis results to observe the time frame it outputs. It makes sense that the output frames after applying these reasonable parameters would identify frames during a time of dispersion and stability. The ten output frames are all adjacent to one another, indicating a potential optimized point of time in the cloud of uniformity.

These parameters have not been calibrated in a way to determine any particular desired cloud, but instead provide a proof of concept to what the methodology is capable of. Calibrating correct threshold parameters would include further testing and requirements for an output, which is not the purpose of this study, but could be applied in future applications.

# 5 CONCLUSION AND FUTURE RECOMMENDATIONS

The objective of this thesis was to develop a methodology of understanding a powder cloud distribution visually through image analysis where quantitative measures are taken from the distribution as it changes with time. Looking at individual frames and analyzing their pixel intensities to estimate dust presence spatially provides insight into the distribution of the dust cloud. Comparing these frames with one another and plotting the intensities as they change across the frames allows more information into the temporal trends of the dust cloud within a video.

Providing input parameters also allows all the measurement data to be assessed and for the process to output frames that must satisfy requirements of the cloud distribution. Applying this process could potentially give insight into the ignition time for future applications in dust explosivity testing as well as if a cloud ever fully reaches a desired state of uniformity. Lawrence Livermore National Laboratory proposed this project as a means for these future applications to take place.

## 5.1 Conclusion

This thesis provides an approach of generating a dust cloud within a transparent enclosure and a setup to acquire high-speed footage of the cloud. Additionally, this thesis produces a valid methodology to quantitatively assess characteristics of dust cloud distribution within an enclosure, including dust presence globally and locally, uniformity through variation across enclosure, and the stability of the cloud all as it changes with time. This is done by segmenting the enclosure into regions and finding the mean intensities, standard deviation, and standard deviation rate of change.

Within this methodology, light attenuation principles by Bouguer-Beer-Lambert Law are applied to estimate the light extinction coefficient from the pixel intensities and the enclosure geometry. Additionally, this process successfully includes a way of applying input parameters to determine the time at which optimized dust cloud distribution is achieved. This is done by

applying thresholds to the dust cloud characteristic data and generating output frames in a video that satisfy the required criteria. With refined, appropriate criteria parameters determined for a specific application of this process, this methodology provides a promising means of determining dust distribution uniformity as it relates to the timing of explosivity ignition or potential other applications.

## 5.2 Limitations

This process uses high-speed footage which consists of images that are a two-dimensional representation of a three-dimensional cloud. Inherent error exists in the approximation that this is representative of the entire cloud since details within the cloud are potentially obscured. Additionally, due to the limited frame rate of the camera setup, the footage lacks a degree of time resolution that would have augmented the accuracy of the analysis results.

The clouds generated by the experimental setup are not uniform which applies further limitations to this project. Using Bouguer-Beer-Lambert's law to estimate the extinction coefficient, $\beta$, at every point in the enclosure is limited with the nonuniformity of the dust cloud. The accuracy of this measurement could improve considerably though improving the uniformity of the cloud. Also, the method to output a frame with an optimized, uniform cloud is not able to be verified without a uniform cloud that acts as a reference.

This methodology's results depend highly on the user's ability to determine the threshold parameters to be applied to the analysis data. Without adequate threshold values for an application, misleading outputs can occur through this method.

## 5.3 Recommendations

Many of the limitations of this study can be mitigated through refining the experimental setup. The most robust way to validate this methodology would be with a setup that produces a controlled, uniform cloud. This would likely involve turning away from metal AM powders

altogether, in favor of an attenuating medium that has buoyancy effects, such as smoke, that could uniformly distribute inside the vessel. A setup like this would then permit a more fine-tuned control over the cloud uniformity, which could address and resolve the unknowns in this method. After this is concluded, the method could then be confidently applied to non-uniform AM powder clouds with an increased understanding into the effects of cloud uniformity.

Footage acquisition improvements could include using a DC backlight source that would eliminate the flickering effect, allowing faster frame rates. It is recommended to increase the frame rate significantly to improve the time resolution of the data set. It is also important to have adequate backlighting in the testing setup to provide strong contrast with dust particles in a cloud. Consistent backlighting diffusion is recommended as it reduces effects of hotspots and any areas of overexposure. Using a monochromatic backlight also improves the application of BBL law by following the assumptions more accurately.

Eliminating as much ambient light while taking footage is beneficial for the application of the BBL law as well as not having glares on the enclosure. Any light that is not produced by the backlight in the frames, is considered ambient light and does not aid in the determination of dust presence in a frame. A process that may help determine the ambient light that exists in a future test setup would be to completely block the backlight source by a dark panel and then use the pixel intensity that still exists in the corresponding frames to be attributed to the ambient light. This intensity with the light blocked could be used as the lower limit of the pixel intensity, corresponding to dust blocking 100% of the light which could scale the intensity values more accurately.

A recommendation for future research that may improve the two-dimensional representation of a three-dimensional cloud would be to add another high-speed camera during footage acquisition and cloud generation. Employing another camera that views another perspective of the same dust cloud would provide more information of the uniformity in multiple views. Information from each camera's corresponding frame could be compared and assumptions

could be assessed and improved in the analysis. For example, having two cameras facing perpendicular to one another could improve the path length value used in the extinction coefficient, β, calculation so that the distance used as the path length represents the actual cloud distance (measured by the perpendicular camera footage) rather than the distance the cloud *could* take up. Additionally, applying the analysis and criteria on both camera's footage independently and then comparing if the results match gives further insight on the clouds uniformity than just using one camera.

# REFERENCES


[1] W. E. Frazier, "Metal Additive Manufacturing: A Review," *Journal of Materials Engineering and Performance*, vol. 23, 2014.

[2] "Combustible Dust Hazard Study," U.S. Chemical Safety and Hazard Investigation Board, 2006.

[3] N. S. Reding and M. B. Shiflett, "Metal Dust Explosion Hazards: A Technical Review," *Industrial & Engineering Chemistry Research*, vol. 57, pp. 11473-11482, 2018.

[4] K. L. Cashdollar, "Overview of dust explosibility characteristics," *Journal of Loss Prevention in the Process Industries*, vol. 13, no. 3-5, pp. 183-199, 2000.

[5] K. L. Cashdollar, O. Kalejaiye, P. R. Amyotte and M. J. Pegg, "Effectiveness of dust dispersion in the 20-L Siwek chamber," *Journal of Loss Prevention in the Process Industries*, vol. 23, no. 1, pp. 46-59, 2010.

[6] "20-Liter Sphere Apparatus," ANKO, 2016. [Online]. Available: http://anko-lab.com/en/a/20-liter-sphere-apparatus. [Accessed 2021].

[7] K. L. Cashdollar, I. Liebman and R. S. Conti, "Three bureau of mines optical dust probes," U.S. Bureau of Mines, 1981.

[8] A. Di Benedetto, P. Russo, R. Sanchirico and V. Di Sarli, "CFD simulations of turbulent fluid flow and dust dispersion in the 20 liter explosion vessel," *AIChE Journal*, vol. 59, no. 7, pp. 2485-2496, 2013.

[9] B. Du, W. Huang, L. Liu, T. Zhang, H. Li, Y. Ren and H. Wang, "Visualization and analysis of dispersion process of combustible dust in a transparent Siwek 20-L chamber," *Journal of Loss Prevention in the Process Industries,* vol. 33, pp. 213-221, 2015.

[10] B. Daumann, A. Fath, H. Anlauf and H. Nirschl, "Determination of the mixing time in a discontinuous powder mixer by using image analysis," *Chemical Engineering Science,* vol. 64, pp. 2320-2331, 2009.

[11] P. Bedggood and A. Metha, "Mapping flow velocity in the human retinal capillary network with pixel intensity cross correlation," *PloS One,* vol. 14, no. 6, pp. e0218918-e0218918, 2019.

[12] Y. Zhao and K. R. Ambrose, "A Real-time Method for Sensing Suspended Dust Concentration from the Light Extinction Coefficient," *Journal of Loss Prevention in the Process Industries,* vol. 67, 2020.

[13] C. C. f. R. Sensing, "Fundamentals of Remote Sensing," Canada Centre for Mapping and Earth Observation, 2019.

[14] R. A. Ogle, Dust Explosion Dynamics, 2016: Elsevier Science and Technology.

[15] S. Grenley, "Extinction Coefficient Measurement Comparison of Tungsten Powder Clouds," M.S. Thesis, College of Eng. Cal Poly State Univ., San Luis Obispo, 2021.

# APPENDICES

## *A. TESTING EQUIPMENT DETAILS*

Table 5-1. Testing Equipment and Material Details.

| Equipment/Material | Purpose | Notes |
|---|---|---|
| Acrylic Tube 10-inch OD x 9-3/4 inch ID | Containment walls of enclosure | Cut to 24-inch height |
| Acrylic sheet | Top lid of enclosure | Laser cut into 12-inch diameter circle and 12-inch diameter ring |
| Polyethylene plastic pan 17-inch diameter | Bottom dust collection pan | |
| Polyurethane rubber sheet | Sealing ring to keep dust from leaking out | Cut into rings and sandwiched between acrylic top lids and clamped |
| 8-inch diameter test sieve W.S. Tyler -0.075mm, 0.106mm, 0.150mm | Disperse powder into a cloud | Best mesh size with tungsten powder was 0.075mm Grounded with clamped wire on rim |
| 40 mm t-slot framing | Frame to connect to enclosure and be structural | |
| Micro Metal Geared 6V motor | Rotate cams to tap sieve in powder release | Powered with 5 V |
| 22-gauge wire | Connect the motors to 5V power supply | |
| PLA 3D print filament for frame connections | Connect t-slot frame together<br>Connect frame to enclosure<br>Ring to support testing sieve<br>Mount motor to cylinder walls<br>Create cams to tap sieve | 3D printed using a Prusa printer |
| Phantom v310 high-speed camera | Acquire high-speed footage | |
| Sigma Zoom 24-70 mm 1:2.8 EX DG Macro 82 mm Lens | Interface with high-speed camera to acquire footage | |
| CoolStar florescent bulb FV-CFL150120 | Provide light for image acquisition | Diffuse in a soft box |
| Licron Crystal™ Permanent Clear Static Dissipative Coating | Provide antistatic properties for acrylic | Creates hazy finish unless professionally applied—did not use for enclosure but has potential |

## *B. ALTERNATE CLOUD FORMATION TEST DESIGNS*

### Obstacle Drop Test

- Manually operated trap door holding the powder above the enclosure
- Obstacle fixed in the enclosure to collide with the falling powder and disperse it into a cloud formation.
- **Pros:**
  - •Obstacle can easily be removed and exchanged for different designs depending on cloud produced
  - •Straightforward build
- **Cons:**
  - •Unsure of applicable cloud formation
  - •Potential dead zone below obstacle and supports

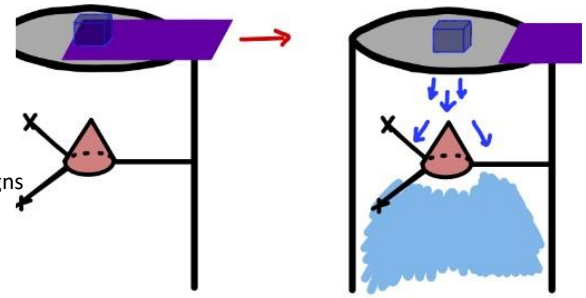

### Sieve Drop Test

- Concave sieve tohold powder
- Manually operated movement fosieve throughenclosure from the side (or the top)
- Flexible attachments for sieve
- **Pros:**
  - Potentially more homogeneous cloud
  - Minimizes dead space
  - Straightforward build
- **Cons:**
  - Unsure of applicable cloudformation
  - Might be difficult to keep powder from falling before test
  - Inconsistent and slow test

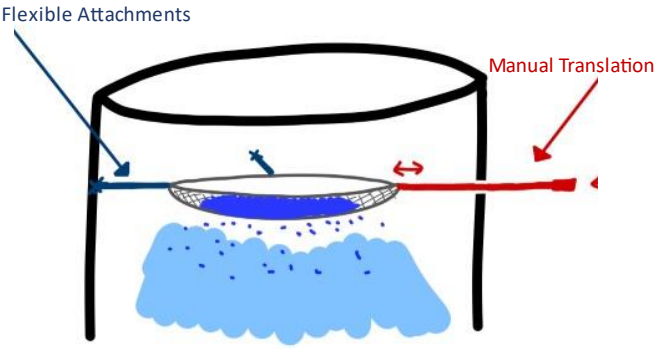

## Spinning Dispersion Tests

- Spinning devices could consist of a conical shape or a disk that flings dust out and would rebound off the enclosure to create a dust cloud
- **Pros:**
  - Uses less space than a drop test
  - Could potentially replicate the desired dust cloud after rebound
- **Cons:**
  - May just shoot directly at enclosure walls and slide down
  - Necessitates a powerfulactuator (maybe even a pneumatic dremel)

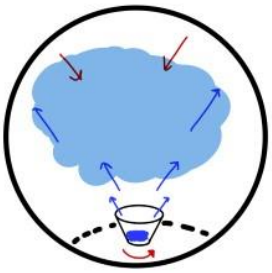

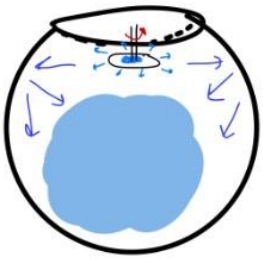

## Refined Spinning Dispersion Design

- Conical device holds powder inside until actuated to rotate
- Powder flings upward and rebounds off stationary disk above
- Rebound disk could be designed with curvature and ridges to give the powder different rebound angles
- **Pros:**
  - Emulates similar rebound path as the desired pressure vessel test
  - Could iterate designs for the rebound disk to get desired cloud formation
- **Cons:**
  - May have a dead zone below disk with no powder cloud
  - Necessitates a powerfulactuator
  - More complicated design and build

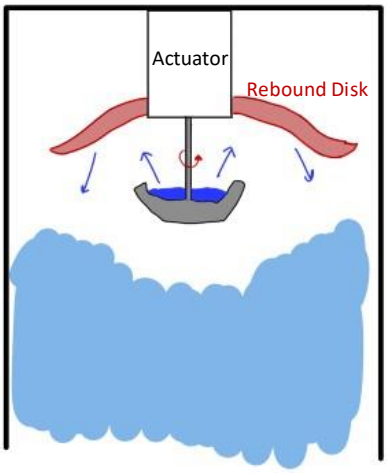

## Compressed Air Burst Design

- "Shelf" lining the perimeter of the cylindrical enclosure with hose attached on top connected to compressed air
- Hose has orfices equally spaced apart to allow air to blow through into the enclosure
- Powder is placed in equal amounts directly in front of the orfices to be blown off into the enclosure when actuated
- **Pros:**
  - Variable air pressure to produce different clouds
  - Straightforward build
- **Cons:**
  - May force powder in the center with undesired dispersion in the enclosure
  - Involves more powder handling than other designs
  - Would need to be vented

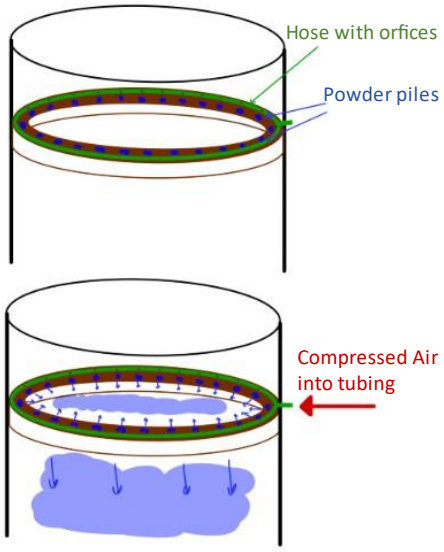


## C. *TEST PROCEDURE & SAFETY GUIDELINES*

### Thesis Test Procedure and Safety Guidelines

Process:

Create a tungsten metal powder cloud in a testing enclosure.

Purpose:

During the period of Fall, Winter, and Spring quarter of 2020/2021, Shelby Lampshire and Spencer Grenley will be completing a series of tests to generate data for their master's thesis. The testing goal is to replicate a tungsten powder dust cloud in a transparent, sealed enclosure in order to get high speed footage and optical density probe measurements.

Testing Enclosure Design:

The testing enclosure includes a transparent cylinder with a top and bottom attached to a t-slot frame sitting on a table. At the top of the cylinder, a suspended testing sieve would hold tungsten metal powder. A mechanism will release the powder while inside the sealed enclosure. This will cause the powder to fall through the sieve and create a cloud.

During testing, both top and bottom of the enclosure will be sealed to keep any dust from entering the surroundings. The bottom includes a collection pan for the powder to fall into that is held up against the bottom of the cylinder by the frame. When testing is finished and the powder has settled, the frame can be loosened to allow the pan to lower and the powder to be put back into its storage container.

The top of the cylinder is sealed with a flange, rubber ring, and acrylic plate sandwiched and clamped together.

Work Area:

The area that has been approved for work on these theses is at Cal Poly in 13-126. No other people will be working in this lab during Fall and Winter quarter.

Figure 5-1. Provided workspace for thesis testing at Cal Poly San Luis Obispo.

Materials and Set Up:

The set up for the test will include a sealed transparent enclosure that will contain the metal powder cloud created during testing. This will sit on a flat surface along with a lighting set up and a nearby high-speed camera set up.

The material intended for the test is tungsten metal powder with a particle size averaging 38 μm in diameter. The powder is intended to be kept dry and sealed for the duration of testing.

Approximately 2 kg of this tungsten powder will be supplied by Lawrence Livermore National Laboratory (LLNL) for testing purposes.

Metal Powder Handling and Storage

Any handling of metal powder will be done in a well-ventilated space with proper PPE. (See risk mitigation section below)

The proper storage of tungsten powder will be followed according to Lawrence Livermore National Lab's procedures. This will be available for this project soon.

Test Procedure:

1. Open rolling door to allow ventilation in the testing space.
2. Make sure enclosure is clean and sealed at the bottom with its collection system in place.
3. Take off top seal of enclosure and assemble the test sieve to fasteners, grounded wire, and motion arm.
4. Set up camera.
5. Make sure all PPE is on.
6. Take out powder from container and weigh amount needed for test (TBD how much powder)
7. Transfer powder into testing sieve as evenly as possible (some may drop through which is to be expected) Do not shake sieve.
8. Seal top of enclosure.
9. Close rolling door to eliminate outside light for glare.
10. Set up lighting and exposure and start camera
11. Perform test: shake outside arm to allow sieve to let the metal powder fall through until empty.
12. Stop camera filming.

13. Open rolling door.
14. Allow dust to entirely settle inside enclosure- maybe 15 minutes
15. Unseal the bottom collection system and carefully pour powder into storage container and seal.
16. Follow cleaning procedure.

Cleaning Procedure:

After any handling of powder, all surfaces will be wiped down with wet wipes (in accordance with LLNL's recommendations). The wipes will be collected and stored until proper discarding. The sealed collection system at the bottom of the enclosure will collect the bulk of the tungsten powder after the test. Once carefully emptied into the storage container, the interior cylinder walls will be wiped down to collect any leftover powder.

In the case of powder spillage, an antistatic broom will be used to collect the powder and it will be placed in a separate sealed container to be discarded properly.

Waste Disposal

The tungsten powder will be reused for testing, so minimal powder waste should be generated. However, all wipes and used disposable cleaning supplies will be collected and stored safely until a proper disposal process can be completed. (See risk mitigation section below)

Risk Mitigation:

<u>Explosivity Risk:</u> This powder has been tested for explosivity and has **not** been found to be explosive in the form (dry and with stated particle size) stated in the test. On attached Fike Document, see Appendix B, page 5 for reference.

However, the following procedures have been developed to mitigate even the slight risk of flammability or explosivity:

-The powder and testing setup will not be near any ignition or open flame

-The interior surfaces of the transparent enclosure will be coated with Licron Crystal™ Permanent Clear Static Dissipative coating to prevent static buildup during testing. This will not only decrease the dust cloud's tendency to line the surface of the enclosure but also mitigate the risk of any static charge buildup that could cause a spark or ignition during testing.

-The metal sieve has the capability to generate a static charge so we will connect it to a grounding wire to dissipate any charge

Toxicity Risk: The main risk of metal powder handling seems to come from skin to powder contact or inhalation. To mitigate these risks are the follow procedures:

- During any handling of uncontained metal powder, the following PPE will be worn by those in the room:

-Nitrile or chemical resistant gloves

-skin protective clothing (long pants, sleeves or lab coat, closed shoes)

-face shield or safety glasses

-respirator (particulate mask)

-The NIOSH-approved particulate filtering facepiece respirators started with N95 masks and increased in filtration from there, but due to the difficulty of acquiring those masks (Covid) we may have to use KN95 or similar.

-However, according to the CDC website, "Respirators should only be used when engineering control systems (such as adequate ventilation or scrubbing of contaminants) are not feasible. Engineering control systems are the preferred control methods for reducing worker exposures."

- When handling any uncontained metal powder, the large rolling dock door next to our working area will be open to allow adequate ventilation.

- After powder handling, all surfaces and tools will be wiped down to remove any contaminants.

Environmental Hazard Risk:

-The powder will be reused during testing so minimal waste will be produced

-However, a plan for a one-time waste disposal process at the end of testing will need to be developed. This most likely will be include sending the tungsten powder back to LLNL.

## *D. MATLAB SCRIPT*

```
%% grayscale_footage_full_analysis.m
% Description: Applying region analysis to all images in a video.
Applying
% statistical criteria to find optimized frames
% Author: Shelby Lampshire
% Date last modified: 06/19/2021

clearvars;

%% Bring in footage and adjust frame accordingly
Footage = VideoReader('sieve1.avi','CurrentTime', 1.2);
%read in high-speed footage

%set initial (background with no dust) frame number
initial = 2;
frame_uncropped = read(Footage,initial);

%Rotate and crop image to only show enclosure
%manually adjust rotate angle to make enclosure straight before
running
%after running, will need to manually crop image:
    %make sure enclosure is CENTERED
    %crop at edge of enclosure
    %do not crop off sides of enclosure
%if first time applying footage, use command below and comment
out
%"saved_crop" on line 27 and "rot" on line 26 and input rotation
manually and crop manually
%[frame,saved_crop] =
imcrop(imrotate(frame_uncropped,rot,'bilinear','crop'));

rot = -0.5;         %set rotation angle
```

```
saved_crop = [65,5,678,467];

%apply crop and rotation adjustments to uncropped frame
[adjusted_frame,sect] =
imcrop(imrotate(frame_uncropped,rot,'bilinear','crop'),saved_crop
);

figure()
imshow(adjusted_frame)

%% Define enclosure diameter (in inches and pixels)
dia = 9.75;      %interior enclosure diameter (in inches)

%measure adjusted_frame's diameter in pixels using the imtool
command and click measure tool
%click interior cylinder edge point on one side and drag to
interior edge of other side as flat as possible
%remember pixel number and input below in dia_pix

%imtool(adjusted_frame)

dia_pix = 650;      %interior enclosure diameter in adjusted
image (in pixels)

%% define values for analysis:
num_start = 0;    %frame to start the analysis at (before -1)
num_frames = (Footage.NumFrames)-num_start;    %number of frames
analyed

normtype = 'normbeta'; %define normalization method
                       %options:
                       %'normratio', 'normsubtract','normbeta'
i_percentile = 20;  %intensity percentile to set intensity
threshold criteria
sdd_percentile = 35;    %std deviation rate percentile to set SD
rate threshold criteria

%% create regions in enclosure

%region origin values (top left corner of region)
sptr = 10;      %starting row value
sptc = 75;      %starting column value
%pixel distance between region origin values
rspace = 150;   %row direction (x)
cspace = 180;   %column direction (y)

%define region origin values
rows = [sptr sptr sptr sptr+rspace sptr+rspace sptr+rspace
sptr+2*rspace sptr+2*rspace sptr+2*rspace];
cols = [sptc sptc+cspace sptc+2*cspace sptc sptc+cspace
sptc+2*cspace sptc sptc+cspace sptc+2*cspace];
```

```
%define region size values:
w = cspace;          % width of sections
h = rspace;          % height of sections


%% define colormap for plots
c = colormap(lines(length(rows)));      %for some unknown reason
creates empty figure
c(8,:) = [0,.3,0];
c(9,:) = [0.435,0.2,0.184];

%% Create initial frame for all normalization methods

i_frame = imfilter(read(Footage,initial), fspecial('gaussian'));
i_frame =
imcrop(imrotate(i_frame,rot,'bilinear','crop'),saved_crop);
i_frame(i_frame==0)=1;

%% Create path length matrix
path_length = cylpathlength(adjusted_frame,dia,dia_pix);

%% Find region mean, SD, SDD

Mean_sect = zeros(length(rows),num_frames);
for i = 1:num_frames
    %preprocessing steps:
    frame = imfilter(read(Footage,num_start+i),
fspecial('gaussian'));
    frame =
imcrop(imrotate(frame,rot,'bilinear','crop'),saved_crop);
    frame(frame==0)=1;
    [frame_normalized] =
normalizeframe(normtype,frame,i_frame,path_length);
    % finding region intensity(after normalization) means:
    for j= 1:length(rows)
        Mean_sect(j,i) =
(mean2(frame_normalized(rows(j):rows(j)+h,cols(j):cols(j)+w)));
    end
end

%calc the mean norm intensity of ENTIRE frame using region means
Mean_frame = mean(Mean_sect,'omitnan');
%calc the standard deviation bw the region means
SD = std(Mean_sect);

%calc the rate of change of standard devation
SD_dot = zeros(1,num_frames);
deriv_num = 2;    %number of frames to used in stability criteria
to get rate of change across (must be EVEN)
for i = 1:num_frames-deriv_num/2
    if i > deriv_num/2
```

```
        %take adjacent SD values subtracted from one another
(change in SD) and divide by change in time
        SD_dot(i) = abs((SD(i+deriv_num/2)-SD(i-
deriv_num/2))/(deriv_num));
    else
        %slightly change how rate of change is taken to avoid
negative indices
        SD_dot(i) = abs((SD(i+deriv_num)-SD(i))/deriv_num);
    end
end

%% plot the changing average intensity
t = (num_start:num_frames+num_start-1);

legendInfo = [];
f = figure();
f.Position = [10 50 700 500];
hold on;
for n = 1:length(rows)
    legendInfo = [legendInfo; 'Region ',num2str(n)];
    plot(t,Mean_sect(n,:),'linewidth',1.25,'color',c(n,:));
end
xlabel('Frame Number (at 120 fps)');
ylabel('Normalized mean pixel intensity') ;
hold on;
legend(legendInfo, 'Location','southeast');
set(gca,'FontSize',12)


%% apply statistical criteria to frames to find optimized
frame(s)

opt_num = 10;       %number of optimized frames to output
[oframeindex,i_thresh,sdd_thresh]=
apply_stat_criteria(Mean_frame,i_percentile,SD,SD_dot,sdd_percent
ile,opt_num);

opt_frame = imfilter(read(Footage,num_start+oframeindex(1)),
fspecial('gaussian'));
opt_frame =
imcrop(imrotate(opt_frame,rot,'bilinear','crop'),saved_crop);

%show best frame for normalized method
figure()
imshow(opt_frame)
title(sprintf('"best frame" found using %s',normtype));
text(20,20, sprintf('Frame %d', oframeindex(1)+num_start),
'Color', 'w','linewidth',1);
textx = oframeindex(1)+20;
texty = mean(SD);

figure()
```

```
subplot(3,1,1), hold on;
plot(t,Mean_frame, 'k')
yline(i_thresh,'r','linewidth',.75)
hold on;
for i = 1:opt_num
    xline(oframeindex(i)+num_start,'color', [0,0.447,0.741])
end
text(5,i_thresh-.15*i_thresh, sprintf('-? threshold percentile=
%.2d', i_percentile),'color','r','FontSize', 11)
xlabel('Frame Number (at 10000 fps)');
ylabel('Mean -? [1/cm]') ;
set(gca,'FontSize',10)
subplot(3,1,2), hold on;
plot(t,SD,'k')
for j = 1:opt_num
    xline(oframeindex(j)+num_start,'color', [0,0.447,0.741])
end
text(textx,texty, sprintf('Frames %d - %d',
min(oframeindex(:))+num_start,max(oframeindex(:))+num_start),
'Rotation', 90,'color', [0,0.447,0.741])
xlabel('Frame Number (at 10000 fps)');
ylabel('Standard Deviation [1/cm]') ;
set(gca,'FontSize',10)
subplot(3,1,3), hold on;
plot(t,SD_dot,'k');
yline(sdd_thresh,'r','linewidth',.75);
text(5,sdd_thresh+1.2*sdd_thresh, sprintf('SD RoC threshold
percentile= %.2d', sdd_percentile),'color','r','FontSize', 11)
for k = 1:opt_num
    xline(oframeindex(k)+num_start,'color', [0,0.447,0.741])
end
xlabel('Frame Number (at 10000 fps)');
ylabel('SD RoC [1/cm per frame]') ;
set(gca,'FontSize',10)

%% apply a bounding box around sections
figure()
imshow(adjusted_frame,[]);
hold on
for i = 1:length(rows)
    x = cols(i);
    y = rows(i);
    rectangle('Position',[x y w
h],'EdgeColor','k','linewidth',2);
    text( cols(i)+10, rows(i)+20, sprintf('Region %d', i),
'Color', c(i,:),'linewidth',2,'FontSize', 14);
end
title("Regions Used in Analysis");
```

**normalization function:**

```
function [frame_normalized] =
normalizeframe(type,frame,i_frame,pathlengthmatrix)
%Normalize the pixels in an image by the initial background
pixels by
%division, subtraction, or by applying the Bouguer-Beer-Lambert
Law.
%   The first input is the type of normalization technique to
use. This can
%   either be 'normratio', 'normsubtract' or 'normbeta'
%   The second input is the frame to be normalized
%   The thrid input is the initial background frame to be used in
the
%   normalization
%   The fourth input is the path length matrix of the enclosure
which is
%   the same size as the other input frames

if strcmpi(type,'normratio') == 1
    frame_normalized = im2double(frame)./im2double(i_frame);
elseif strcmpi(type,'normsubtract') == 1
    frame_normalized =(im2double(frame)-im2double(i_frame));
elseif strcmpi(type,'normbeta') == 1
    I_ratio = im2double(frame)./im2double(i_frame);
    ln_ratio = log(I_ratio);
    %divide by the path length matrix:
    frame_normalized = ln_ratio./pathlengthmatrix;
else
    error('Error. \n Input 1 not recognized')
end
end
```

**statistical criteria application function:**

```
function [best_frame_index,i_thresh,sd_dot_thresh] =
apply_stat_criteria(mean,i_percentile,std,std_rate,std_rate_perce
ntile,min_num)
%This function outputs the index to the frame that meets all
criteria set
%in the inputs with a minimum standard deviation. This is to
determine the
%frame with best homogeneity
%   The inputs:
    %a mean vector of the mean intensity of each frame
    %the percentile to set the threshold for the intensity mean
to ensure enough dust is present in frame
    %a standard deviation vector of the std value of each frame
    %a standard deviation rate of change vector
```

```
    %the percentile to set the threshold for the std rate of
change to ensure stability around the frame
    %the number of best frame values to output

%criteria 1: intensity low enough to ensure there is enough dust
present
i_thresh = prctile(mean,i_percentile);      %set intensity thresh
to be a percentile of mean intensity data

% apply criteria 1 to generate a range of frames where intensity
is low
range_i = find(mean<i_thresh);

%criteria 2: standard deviation is not fluctuating much (low sd
rate of change)
%set sd_dot threshold to be a low percentile of all rate of
change points
sd_dot_thresh = prctile(std_rate(range_i),std_rate_percentile);

% apply criteria 2 to generate a range of frames where this is
met
range = find(std_rate(range_i)<sd_dot_thresh);
range = range_i(range);     % change index of range to match
index of range_i = index of input vectors & frames
% criteria 3: find frame in range with minimum standard deviation
bw sections
min_sd = mink(std(range),min_num);

%find index for where minimum SD was found to match with footage
frames to output
for i = 1:min_num
    if i<=length(min_sd)
        best_frame_index(i) = find(std==min_sd(i));
    else
         best_frame_index(i) = NaN;
    end

end
```

**Cylinder path length function:**

```
function [cyl_pathlength] =
cylpathlength(adjusted_im,dia_inch,dia_pix)
%Create a path length matrix for a cylindrical enclosure
%   First input is an image/matrix the same size that the path
length needs to be
```

```
%   Second input is the diameter of the enclosure in inches
%   Third input is the diameter of the enclosure in pixels


d = dia_inch*2.54;      %interior enclosure diameter converted to
cm
r = d/2;                %radius in cm
r_pix = dia_pix/2;      %pixel amount of radius
h = d/dia_pix;          %conversion of 1 pixel to scale in cm

path_length = double(zeros(1, dia_pix+1));
for i = 1:dia_pix+1
    if i == 1 || i == dia_pix+1
        path_length(i) = 0;
    else
        path_length(i) = 2*(sqrt((r^2)-(abs((r_pix+1)-i)*h)^2));
    end
end

% making cylinder matrix

%repeat path length vector vertically to get matrix for the
cylinder
[x_size, y_size] = size(adjusted_im);    %acquire desired frame
dimensions
cyl_pl = ones(x_size, length(path_length));
cyl_pl = cyl_pl.*path_length;

%pad array with zero columns to get same array dimensions as
cropped frame
%check if number of columns needed to add is even or odd
%if even, just pad both sides equally to get desired dimensions
%if odd, pad unevenly (left side gets one more padded column) to
get desired dimensions
a = (y_size-length(path_length));
pad = round(a/2);
if a>=0 && dia_pix>0
    if mod(a, 2) == 0 %even 'a'
        cyl_pathlength = padarray(cyl_pl,[0 pad],NaN,'both');
    else
        cyl_pathlength = padarray(cyl_pl,[0 pad],NaN,'both');
        cyl_pathlength=cyl_pathlength(:,1:end-1);   %delete extra
column at end
    end
elseif a == -1
    cyl_pathlength =cyl_pl(:,1:end-1);   %delete extra column at
end
else
    error('Error. \nInput pixel diameter must be within frame
size and a positive integer')
end
```

```
% set all zeros in the path length matrix to NaN since they will
not
% generate a kc value regardless and dividing by zero will result
in errors
cyl_pathlength(cyl_pathlength==0)=NaN;

end
```

**spherical enclosure path length function:**

```
function [sphere_pathlength] =
spherepathlength(adjusted_im,dia_inch,dia_pix)
%Create a path length matrix for a spherical enclosure
%   First input is an image/matrix the same size that the path
length matrix must be
%   Second input is the diameter of the enclosure in inches
%   Third input is the diameter of the enclosure in pixels

d = dia_inch*2.54;      %interior enclosure diameter (in cm)
r = d/2;                %radius in cm
r_pix = dia_pix/2;      %pixel amount of radius
h = d/dia_pix;          %conversion of 1 pixel to scale in cm

path_length_dia = double(zeros(1, dia_pix+1));
for i = 1:dia_pix+1
    if i == 1 || i == dia_pix+1
        path_length_dia(i) = 0;
    else
        path_length_dia(i) = 2*(sqrt((r^2)-(abs((r_pix+1)-
i)*h)^2));
    end
end
clearvars i

% create radius path length vector
path_length_radius = path_length_dia./2;

% making spherical matrix from path length radius vector at
center
sphere_pathlength = double(zeros(dia_pix+1, dia_pix+1));
pix_rad = path_length_radius./h;        %path length vector for
radius in pixels
for i = 1:dia_pix+1
    r = pix_rad(i);
    for j = 1:dia_pix+1
        if j < (r_pix+1)-r || j > (r_pix+1)+r
            sphere_pathlength(i,j) = 0;
        elseif j >= (r_pix+1)-r && j <= (r_pix+1)+r
```

```
            sphere_pathlength(i,j) = 2*(sqrt(abs(((r*h)^2)-
(abs((r_pix+1)-j)*h)^2)));
        end
    end
end
clearvars i j

%pad array with NaN columns to get same array dimensions as
cropped frame
%check if number of columns needed to add is even or odd
%if even, just pad both sides equally to get desired dimensions
%if odd, pad unevenly (left side gets one more padded column) to
get desired dimensions
%this assumes side edges are included in frame so deleting of
columns in matrix will not be nec.

[row_size, col_size] = size(adjusted_im);    %acquire desired
frame dimensions
diff_row = (row_size-length(path_length_dia));
diff_col = (col_size-length(path_length_dia));

pad_row = round(diff_row/2);
pad_col = round(diff_col/2);

if diff_row>=0 && diff_col>=0 && dia_pix>0
    sphere_pathlength = padarray(sphere_pathlength,[pad_row
pad_col],NaN,'both');
        if mod(diff_row, 2) ~= 0 %odd 'diff_row'
            sphere_pathlength=sphere_pathlength(1:end-1,:);
%delete extra row at end
        end
        if mod(diff_col, 2) ~= 0 %odd 'diff_col'
            sphere_pathlength=sphere_pathlength(:,1:end-1);
%delete extra column at end
        end
elseif diff_row < 0 && diff_col>=0 && dia_pix>0
    sphere_pathlength = padarray(sphere_pathlength,[0
pad_col],NaN,'both');
    sphere_pathlength=sphere_pathlength(1:end-abs(diff_row),:);
%delete extra rows at end
        if mod(diff_col, 2) ~= 0 %odd 'diff_col'
            sphere_pathlength=sphere_pathlength(:,1:end-1);
%delete extra column at end
        end
elseif diff_col == -1
    sphere_pathlength =sphere_pathlength(:,1:end-1);   %delete
extra column at end
else
    error('Error. \nInput pixel diameter must be within frame
size and a positive integer')
end
```

```
%set all zero values around enclosure to NaN to avoid division by
zero issues:
sphere_pathlength(sphere_pathlength<.0001)=NaN;

end
```